Supporting Information

Visible-Light-Driven Ruthenium-Catalyzed Hydrogenation of Manganese Nitride Complex to Ammonia under Ambient Conditions

Yasuomi Yamazaki,[†] *Qiubo Wang,*[†] *Yoshiaki Tanabe,*[†] *Yoshiaki Nishibayashi* [†,*]

[†] Department of Applied Chemistry, School of Engineering, The University of Tokyo, 7-3-1 Hongo, Bunkyo-ku, Tokyo 113-8656, Japan

*Corresponding Author's Email Address: ynishiba@g.ecc.u-tokyo.ac.jp

<Table of contents>

1. General methods S3
2. Photocatalytic reactions S5
    2.1. General procedures S5
    2.2. Time courses of photocatalytic reactions S6
    2.3. Light ON/OFF experiments S11
    2.4. Kinetic study of photocatalytic reactions S12
    2.5. Quantum yields for photocatalytic ammonia production S12
    2.6. Photocatalytic ammonia formation using the ^{15}N-labeled nitride complex S13
    2.7. Isolation of dimanganese complex from reaction solution after photocatalysis S15
    2.8. Analysis of reaction solution after photocatalysis S16
    2.9. Reproduction of **1a** from **4** obtained after the photocatalytic reactions S18
    2.10. Investigation on interaction between complex **4** and [LutH]OTf S20
    2.11. Photocatalytic ammonia formation under low partial pressure of dihydrogen S22
3. X-ray crystallography S24
4. Photophysical and photochemical properties S26
    4.1. General methods S26
    4.2. Photophysical properties S27
    4.3. Stern-Volmer analysis S31
5. Cyclic voltammetry S34
    5.1. General procedures S34
    5.2. Cyclic voltammograms S34
    5.3. Estimation of effective BDFE values S41
6. Investigation on interaction between **^{15}N-1a** and [LutH]OTf S42
7. Supplementary references S44

1. General methods

^{1}H NMR (400 MHz), ^{31}P{^{1}H} NMR (162 MHz), and ^{15}N NMR (29 MHz) spectra were recorded on a JEOL ECS-400 spectrometer in a suitable solvent, and spectra were referenced to residual solvent (^{1}H) or external standard (^{31}P{^{1}H}: 85% H_3PO_4). Elemental analyses were performed at the Microanalytical Center of The University of Tokyo. All manipulations were carried out under an atmosphere of nitrogen or argon by using standard Schlenk techniques or glovebox techniques unless otherwise stated. The gas cylinders containing a mixed gas of dinitrogen and dihydrogen in certain ratios (N_2:H_2 = 80:20 and 95:5 v/v) were purchased from TOKYO KOATSU Co., Ltd. and SUZUKI SHOKAN Co., Ltd., respectively.

The manganese complexes (**1a**,[1,2] **1b**[3]), the catalysts for dihydrogen oxidation (**[2a-H]**OTf,[4] **[2a]**$(OTf)_2$,[4] **[2b]**$(OTf)_2$,[4] **[2c]**$(OTf)_2$,[5] **[2d]**OTf[6]), the photosensitizers (**3a**,[7] **3b**,[7] **3c**,[7] **[3d]**ONf,[8] **[3e]**$(ONf)_2$[8]), the salen ligand bearing chloride substituents ((*R*,*R*)-*N*,*N*'-bis(3-*tert*-butyl-5-chlorosalicylidene)-1,2-cyclohexadiimine, **^{Cl}Salen**)[9] and proton mediators ([ColH]OTf,[10] [LutH]OTf,[11] [PicH]OTf[10]) were synthesized according to the literature. **1c** was synthesized in a manner similar to that of **1a**[1,2] using **^{Cl}Salen** instead of (*R*,*R*)-*N*,*N*'-bis(3,5-di-*tert*-butylsalicylidene)-1,2-cyclohexadiimine (*vide infra*). The ^{15}N-labeled complex (**^{15}N-1a**) was synthesized in a manner similar to that of **1a** using $^{15}NH_4Cl$ instead of $^{14}NH_4Cl$.[1,2] The deuteride complex (**[2a-D]**OTf) was synthesized in a manner similar to that of **[2a-H]**OTf, using D_2 instead of H_2.[4] The lutidinium salt bearing deuterium ion ([LutD]OTf) was synthesized in a manner similar to that of [LutH]OTf, using DOTf instead of HOTf.[11]

Tetrahydrofuran (THF), diethylether (Et_2O), CH_2Cl_2, and hexane were used after the purification of Super Anhydrous Grade Solvents (Super^2 plus series, Kanto Chemical Co., Inc.) with a purification system (Glass Contour). Benzene was used after thoroughly sparging with dinitrogen gas to a super-dehydrated-grade solvent (FUJIFILM Wako Pure Chemicals).

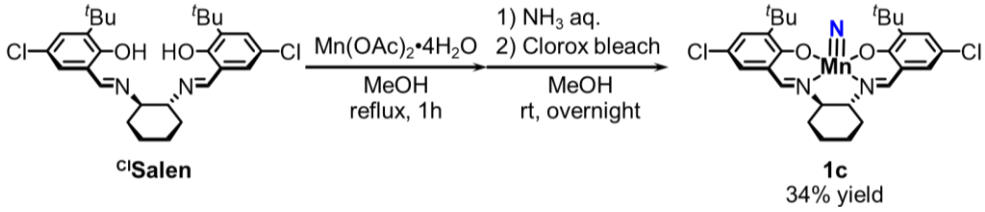

Synthesis of **1c**. **1c** was prepared according to the reported methods[1,2] with the following modifications: In a 500-mL eggplant flask, ^{Cl}**Salen** (5.02 g, 10.0 mmol) was dissolved in 300 mL of MeOH, and the mixture was heated at reflux. $Mn(OAc)_2$•$4H_2O$ (2.58 g, 10.5 mmol) was then added to the yellow solution. The resulting dark brown solution was heated at reflux for 1 h, and then the contents were stirred for 0.5 h at room temperature. Ammonium hydroxide (ca. 6 M in water, 35 mL, 210 mmol) was then added dropwise over 5 min. The solution was stirred at room temperature for 0.5 h. To the vigorously stirring mixture, Chlorox Bleach (ca. 0.7 M of NaOCl aq., 140 mL, 98 mmol) was added dropwise over 40 min. The resulting mixture was stirred at room temperature overnight. The precipitate was collected by filtration with Celite and was washed with MeOH. The solid on the Celite was dissolved in CH_2Cl_2, and the solvent of the CH_2Cl_2 solution was removed under reduced pressure. The obtained solid was purified by silica gel column chromatography (eluent: CH_2Cl_2). After removing the solvent under vacuum, **1c** was obtained as green solids. Yield: 1.94 g, 34%. ^{1}H NMR (400 MHz, CD_2Cl_2): δ 7.96 (s, 1H), 7.91 (s, 1H), 7.31 (d, J = 2.4 Hz, 1H), 7.29 (d, J = 2.4 Hz, 1H), 7.14 (d, J = 2.8 Hz, 1H), 7.09 (d, J = 2.8 Hz, 1H), 3.56-3.53 (m, 1H), 3.05-3.00 (m, 1H), 2.65-2.63 (m, 1H), 2.50-2.47 (m, 1H), 2.02-2.01 (m, 2H), 1.58-1.46 (m, 3H), 1.43 (s, 9H), 1.41 (m, 1H), 1.38 (s, 9H). Elemental Anal. Calcd. (%) for $C_{28}H_{34}Cl_2MnN_3O_2$: C, 58.96; H, 6.01; N, 7.37. Found (%): C, 58.85; H, 5.98; N, 7.05. Recrystallization from CH_2Cl_2 solutions layered with MeOH yielded green needle crystals suitable for X-ray analysis.

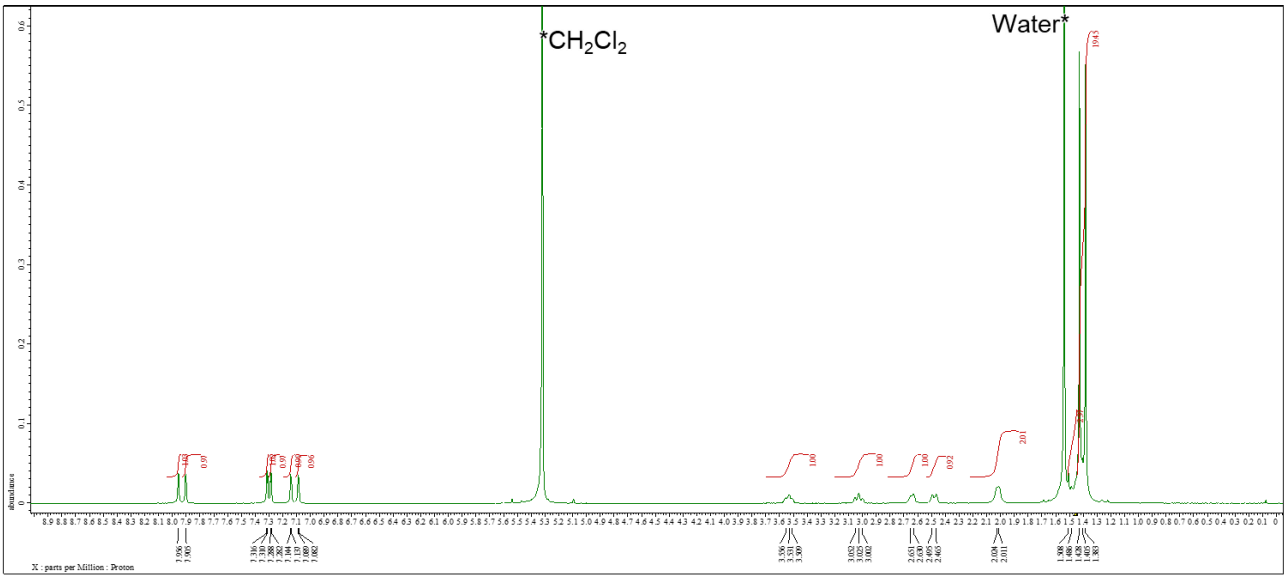

Figure S1. ^{1}H NMR spectrum of **1c** in CD_2Cl_2.

2. Photocatalytic reactions

2.1. General procedures

A typical experimental procedure for the photocatalytic reaction is described below. To a 20 mL Schlenk flask (the volume inside the flask containing the headspace is 31 mL, Figure S2b), **1a** (61 mg, 100 μmol), [**2a-H**]OTf (1.0 mg, 1.0 μmol), and [LutH]OTf (6.6 mg, 25 μmol) were added in a glove box filled with argon gas. After taking the flask out of the glove box, the atmosphere in the flask was changed to dihydrogen. **3a** (6.6 mg, 10 μmol) and THF (5 mL) were then added to the flask under a positive flow of dihydrogen gas. The flask was sealed with a ground-glass cock coated with vacuum grease and sonicated for approximately 10 minutes to prevent the complexes from remaining unsolved. When we analyzed the headspace atmosphere by gas chromatography prior to photoirradiation, no air contamination was observed. The solution was irradiated for 24 hours with four types of LED light (λ = 405, 430, 530, and 590 nm) in a merry-go-round irradiation apparatus (Cell System Co., Ltd., Iris-MG-S, Figure S2a). The solution was stirred by a magnetic stirrer during the photolysis. The inside of the apparatus was continuously cooled by a motor fan to maintain the temperature within 5 °C of room temperature. When the hydrogenation reaction proceeded efficiently, the solution color was changed from orange to green during the photoirradiation (Figure S2c). After the reaction, the reaction solution was evaporated in vacuo, and the distillate was trapped in a dilute H_2SO_4 solution (0.5 M, 10 mL). In the case of the reaction shown in Figure 1 of the manuscript, 75 ± 6 μmol of ammonia was observed, meaning that most ammonia produced was successfully collected at this stage. To the residue in the flask, an aqueous potassium hydroxide solution (30 wt%, 5 mL) was added to convert the ammonium salts produced by the reaction between ammonia and $[LutH]^+$ back into ammonia. Then, the mixture was evaporated in vacuo, and the distillate was trapped in another dilute H_2SO_4 solution (0.5 M, 10 mL). The amounts of ammonia present in the H_2SO_4 solutions were determined by the indophenol method.[12] In the case of the reaction shown in Figure 1 of the manuscript, a total of 80 ± 4 μmol of ammonia was detected, meaning that approximately 75 μmol of ammonia and 5 μmol of ammonium salts were in the reaction solution.

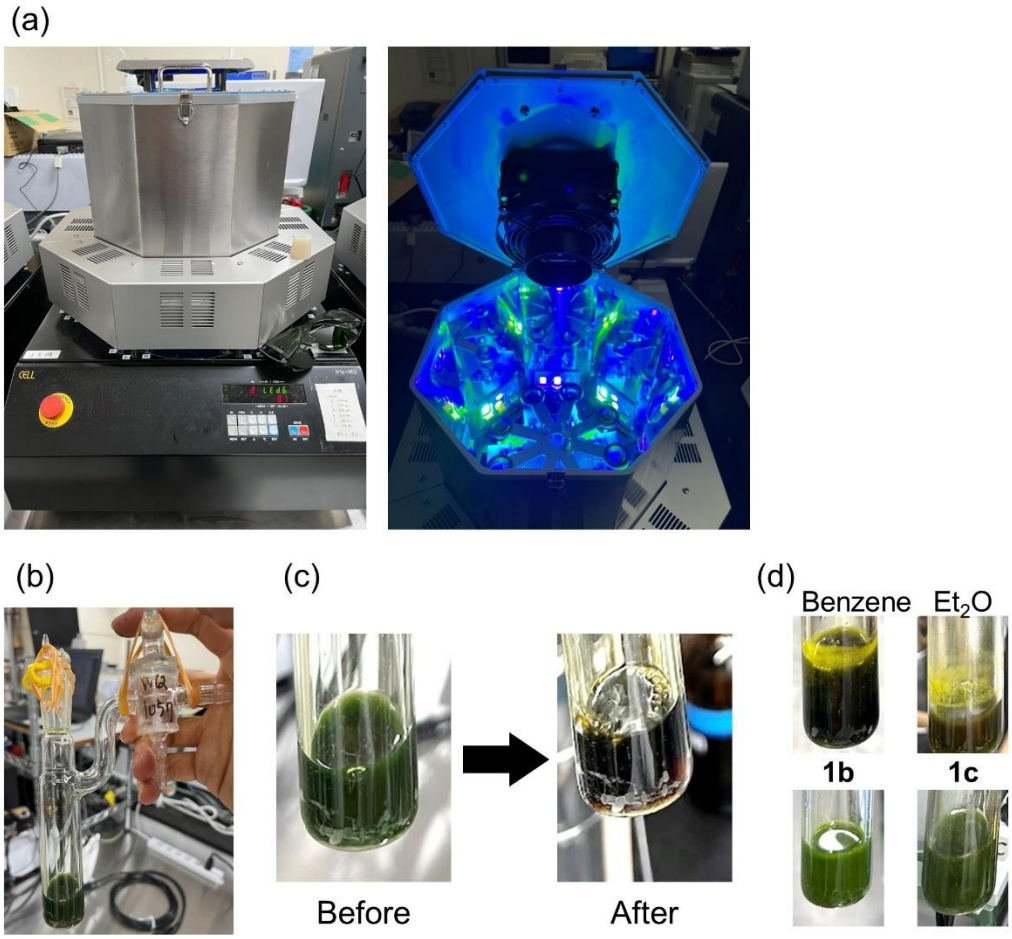

Figure S2. Photographs of (a) the merry-go-round type photo-irradiation apparatus used in this study (CELL System Co., Iris-MG-S) and (b) the Schlenk flask used. The solution color change under the reaction condition shown in Figure 1 of the manuscript is shown in (c). (d) The suspensions after photocatalytic reactions in benzene or Et_2O (Table 2 entries 19 and 21 in the manuscript) and before photocatalytic reactions with **1b** or **1c** (Table 2 entries 22 and 23 in the manuscript).

2.2. Time courses of photocatalytic reactions

Table S1. Photocatalytic hydrogenation of **1a** in the presence of [**2a-H**]OTf, **3a**, and [LutH]OTf: time course of the photolysis.

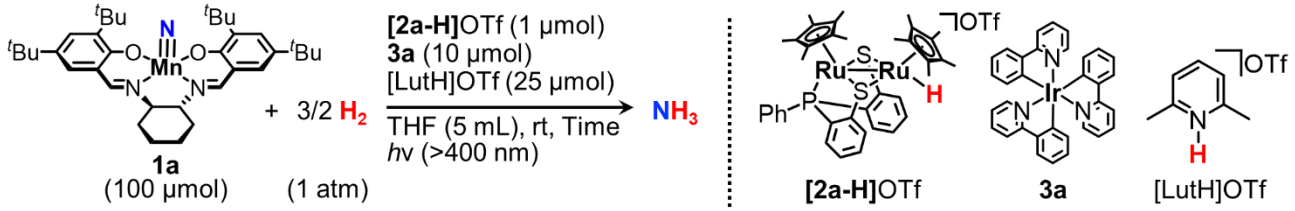

Entry	Irradiation time [h]		NH_3 production [μmol][a,b]	NH_3 yield [%][b,c]
1-1	3		15.2	15.2
1-2	3		14.1	14.1
1-3	3		21.3 (19.7)	21.3 (19.7)
		(Average)	**16.9 ± 2.2**	**16.9 ± 2.2**
2-1	6		39.7 (36.4)	39.7 (36.4)
2-2	6		36.8 (33.6)	36.8 (33.6)
		(Average)	**38.2 ± 1.5**	**38.2 ± 1.5**
3-1	12		51.8	51.8
3-2	12		55.8 (54.5)	55.8 (54.5)
3-3	12		55.0 (53.3)	55.0 (53.3)
		(Average)	**54.2 ± 1.2**	**54.2 ± 1.2**
4-1	24		81.1	81.1
4-2	24		81.4	81.4
4-3	24		68.5 (65.5)	68.5 (65.5)
4-4	24		94.2 (87.3)	94.2 (87.3)
		(Average)	**80.3 ± 4.2**	**80.3 ± 4.2**
5-1	36		77.2	77.2
5-2	36		78.8 (70.9)	78.8 (70.9)
		(Average)	**78.0 ± 0.8**	**78.0 ± 0.8**

[a]The averages are shown with standard errors. [b]The values in the parentheses show the amount of detected free ammonia before addition of the KOH solution. [c]Yield based on **1a**.

Table S2. Photocatalytic hydrogenation of **1a** in the presence of [**2a**](OTf)$_2$, **3a**, and [LutH]OTf: time course of the photolysis.

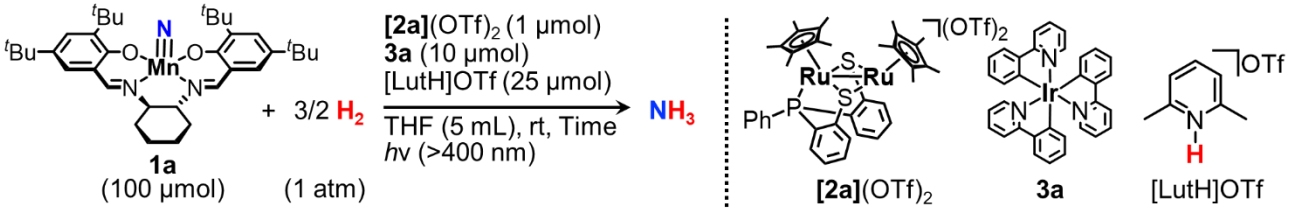

Entry	Irradiation time [h]		NH_3 production [μmol][a,b]	NH_3 yield [%][b,c]
1-1	3		17.5	17.5
1-2	3		17.4	17.4
		(Average)	**17.4 ± 0.1**	**17.4 ± 0.1**
2-1	6		37.6	37.6
2-2	6		33.4	33.4
		(Average)	**35.5 ± 2.1**	**35.5 ± 2.1**
3-1	12		59.5	59.5
3-2	12		53.5 (49.0)	53.5 (49.0)
		(Average)	**56.5 ± 3.0**	**56.5 ± 3.0**
4-1	24		78.5	78.5
4-2	24		80.9	80.9
4-3	24		82.7	82.7
4-4	24		88.1 (80.7)	88.1 (80.7)
		(Average)	**82.6 ± 2.0**	**82.6 ± 2.0**

[a]The averages are shown with standard errors. [b]The values in the parentheses show the amount of detected free ammonia before addition of the KOH solution. [c]Yield based on **1a**.

Table S3. Photocatalytic hydrogenation of **1a** in the presence of [**2b**](OTf)$_2$, **3a**, and [LutH]OTf: time course of the photolysis.

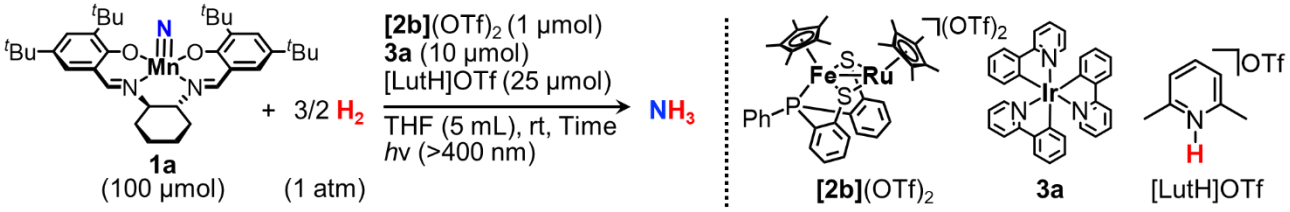

Entry	Irradiation time [h]		NH_3 production [μmol][a,b]	NH_3 yield [%][b,c]
1-1	3		13.7	13.7
1-2	3		16.2	16.2
		(Average)	**15.0 ± 1.3**	**15.0 ± 1.3**
2-1	6		31.7	31.7
2-2	6		39.1	39.1
		(Average)	**35.4 ± 3.7**	**35.4 ± 3.7**
3-1	12		24.5	24.5
3-2	12		41.2	41.2
		(Average)	**32.8 ± 8.3**	**32.8 ± 8.3**
4-1	24		37.5	37.5
4-2	24		30.7	30.7
4-3	24		31.8 (27.6)	31.8 (27.6)
4-4	24		33.7 (31.4)	33.7 (31.4)
		(Average)	**33.4 ± 1.5**	**33.4 ± 1.5**

[a]The averages are shown with standard errors. [b]The values in the parentheses show the amount of detected free ammonia before addition of the KOH solution. [c]Yield based on **1a**.

Table S4. Photocatalytic hydrogenation of **1a** in the presence of [**2c**](OTf)$_2$, **3a**, and [LutH]OTf: time course of the photolysis.

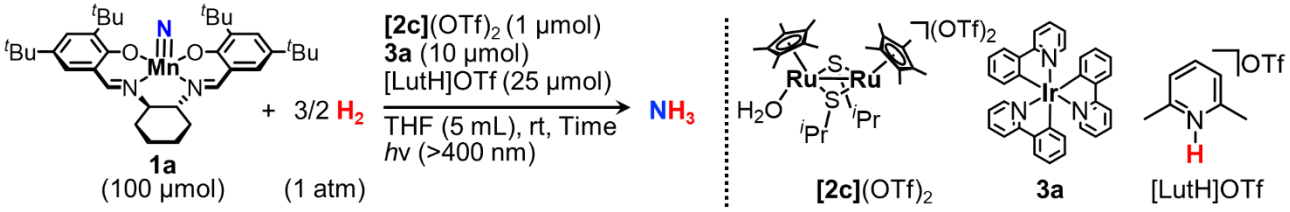

Entry	Irradiation time [h]		NH_3 production [μmol][a,b]	NH_3 yield [%][b,c]
1-1	3		3.9	3.9
1-2	3		1.7	1.7
		(Average)	**2.8 ± 1.1**	**2.8 ± 1.1**
2-1	6		8.7	8.7
2-2	6		5.4	5.4
		(Average)	**7.1 ± 1.7**	**7.1 ± 1.7**
3-1	12		11.1	11.1
3-2	12		8.9 (5.5)	8.9 (5.5)
		(Average)	**10.0 ± 1.1**	**10.0 ± 1.1**
4-1	24		12.3	12.3
4-2	24		12.1	12.1
4-3	24		16.3 (9.4)	16.3 (9.4)
4-4	24		17.0 (9.5)	17.0 (9.5)
		(Average)	**14.4 ± 1.3**	**14.4 ± 1.3**

[a]The averages are shown with standard errors. [b]The values in the parentheses show the amount of detected free ammonia before addition of the KOH solution. [c]Yield based on **1a**.

Table S5. Photocatalytic hydrogenation of **1a** in the presence of [**2d**]OTf, **3a**, and [LutH]OTf: time course of the photolysis.

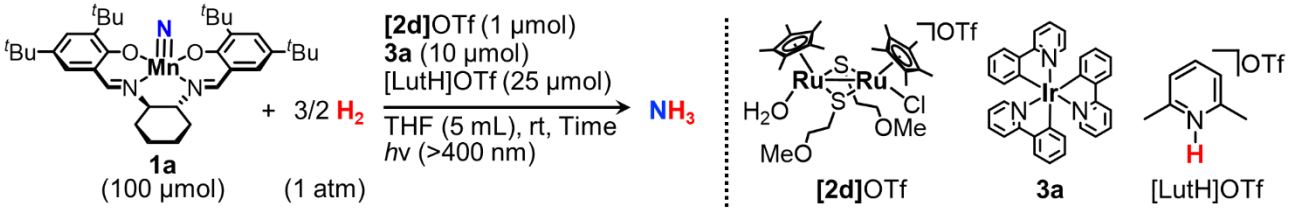

Entry	Irradiation time [h]		NH_3 production [μmol][a,b]	NH_3 yield [%][b,c]
1-1	3		6.1	6.1
1-2	3		2.8	2.8
1-3	3		4.7	4.7
		(Average)	**4.5 ± 1.0**	**4.5 ± 1.0**
2-1	6		3.9	3.9
2-2	6		4.2	4.2
		(Average)	**4.0 ± 0.2**	**4.0 ± 0.2**
3-1	12		7.4	7.4
3-2	12		7.8	7.8
		(Average)	**7.6 ± 0.2**	**7.6 ± 0.2**
4-1	24		6.4	6.4
4-2	24		8.8	8.8
4-3	24		7.9 (6.6)	7.9 (6.6)
4-4	24		8.1 (6.5)	8.1 (6.5)
		(Average)	**7.8 ± 0.5**	**7.8 ± 0.5**

[a]The averages are shown with standard errors. [b]The values in the parentheses show the amount of detected free ammonia before addition of the KOH solution. [c]Yield based on **1a**.

2.3. Light ON/OFF experiments

THF solutions (5 mL) containing **1a** (61 mg, 100 μmol), **[2a-H]**OTf (1.0 mg, 1.0 μmol), **3a** (6.6 mg, 10 μmol), and [LutH]OTf (6.5 mg, 25 μmol) were prepared as described in the general procedures (Section 2.1 in the Supporting Information). The reaction mixture was stirred at room temperature under irradiation (>400 nm) or in the dark (Schlenk flask was wrapped with aluminum foil) for the indicated time. The amount of ammonia was determined by following the general procedures. The results are shown in Table S6.

Table S6. Light ON/OFF experiments for photocatalytic hydrogenation of **1a** in the presence of [**2a-H**](OTf)$_2$, **3a**, and [LutH]OTf.

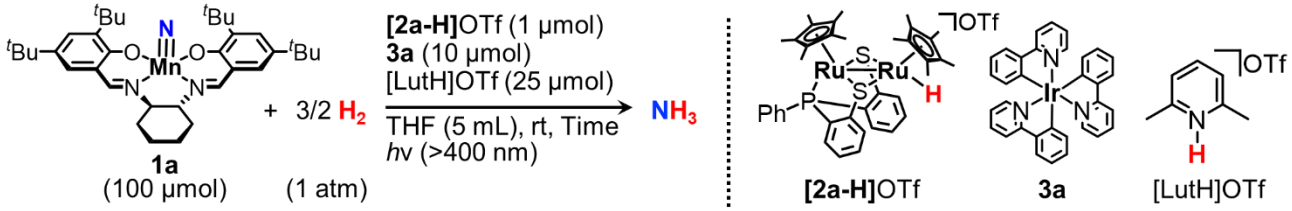

Entry	Light ON/OFF conditions	NH_3 production [μmol][a]	NH_3 yield [%][b]
1	6 h (ON)	38.2 ± 1.5	38.2 ± 1.5
2	6 h (ON)→6 h (OFF)	36.3 ± 0.3	36.3 ± 0.3
3	6 h (ON)→6 h (OFF)→3 h (ON)	46.8 ± 2.6	46.8 ± 2.6
4	6 h (ON)→6 h (OFF)→3 h (ON) →3 h (OFF)	46.9 ± 0.4	46.9 ± 0.4
5	6 h (ON)→6 h (OFF)→3 h (ON) →3 h (OFF)→3 h (ON)	66.2 ± 5.7	66.2 ± 5.7

[a]The averages are shown with standard errors. [b]Yield based on **1a**.

2.4. Kinetic study of photocatalytic reactions

The kinetic isotope effect (KIE) of the catalytic reaction was estimated by measuring the amount of ammonia produced in the catalytic reaction using D_2 instead of H_2. A typical procedure is described below. A THF solution (5 mL) containing **1a** (61 mg, 100 μmol), **[2a-D]**OTf (1.0 mg, 1.0 μmol), **3a** (6.6 mg, 10 μmol), and [LutD]OTf (6.5 mg, 25 μmol) was irradiated (> 400 nm) for 12 h as described in the general procedures (Section 2.1 in the Supporting Information). The amount of ND_3 was determined by following the general procedures. The results of the photocatalytic reactions were summarized in Table S7.

Table S7. Kinetic isotope effect (KIE) of the catalytic reactions.

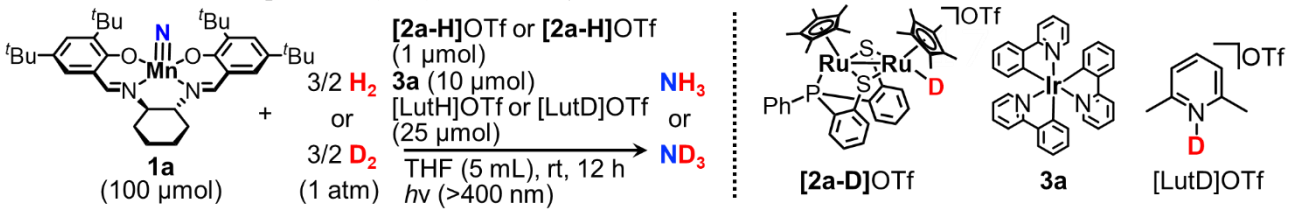

Entry	Atmosphere	NH_3 production [μmol][a,b]	NH_3 yield [%][b,c]
1	H_2	54.2 (53.9) ± 1.2	54.2 (53.9) ± 1.2
2	D_2	17.6 (16.6) ± 0.7	17.6 (16.6) ± 0.7
			KIE = 3.1

[a]The averages are shown with standard errors. [b]The values in the parentheses show the amount of detected free ammonia before addition of the KOH solution. [c]Yield based on **1a**.

2.5. Quantum yields for photocatalytic ammonia formation

The apparent quantum yields for ammonia production ($\Phi(NH_3)$) were determined by measuring the incident photon number from the 405-nm LED light in the merry-go-round irradiation apparatus (Cell System Co., Ltd., Iris-MG-S). The incident photon number was estimated to be 3.3×10^{-7} einstein/s using the chemical actinometer with $K_3[Fe(C_2O_4)_3]$.[13] It should be noted that the estimated apparent quantum yields could be almost the same as internal quantum yields because the reaction solutions contained enough amount of photosensitizers and **1a** to absorb all incident photons. Given that three electrons are required to produce one ammonia molecule, the $\Phi(NH_3)$ value was calculated according to the following equation:

$$\Phi(NH_3) = \frac{3 \times [\text{Produced } NH_3\ (\mu\text{mol})]}{[\text{Incident photons } (\mu\text{einstein})]} = \frac{3 \times [\text{Produced } NH_3\ (\mu\text{mol})]}{3.3\times10^{-7}\ (\text{einstein/s}) \times [\text{Irradiation time (s)}]} \quad \text{(S1)}$$

Table S8. Quantum yields of photocatalytic hydrogenation of **1a** in the presence of [**2a-H**](OTf)$_2$, **3a**, and [LutH]OTf.

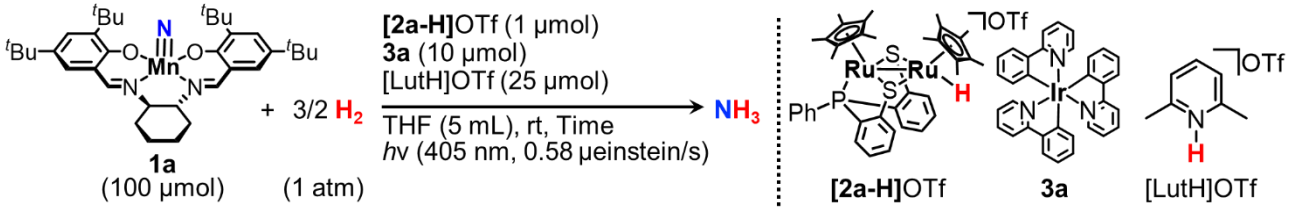

Entry	Irradiation time [h]	Incident photon number [μeinstein]	NH_3 production [μmol]	$\Phi(NH_3)$ [%][a]
1	0.5	598	1.7	0.84
2	1.0	1200	3.5	0.88
			(Average)	0.86 ± 0.02

2.6. Photocatalytic ammonia formation using the ^{15}N-labeled nitride complex

To a 20 mL Schlenk flask, **^{15}N-1a** (62 mg, 100 μmol), [**2a-H**]OTf(1.0 mg, 1.0 μmol), and [LutH]OTf (6.5 mg, 25 μmol) were added in a glove box filled with argon gas. After taking the flask out of the glove box, **3a** (6.6 mg, 10 μmol) and THF (5 mL) were added to the flask under a positive flow of argon gas. The flask was sealed with a ground-glass cock coated with vacuum grease and sonicated for approximately 10 minutes. The solution was irradiated for 24 h with four kinds of LED light (λ = 405, 430, 530, 590 nm) in a merry-go-round irradiation apparatus (Cell System Co., Ltd., Iris-MG-S). The solution was stirred by a magnetic stirrer during the photolysis. The inside of the apparatus was continuously cooled by a motor fan to maintain the temperature within 5 °C of room temperature. After the reaction, the reaction solution was evaporated in vacuo, and the distillate was trapped in a dilute HCl solution (2 M, 10 mL). To the residue in the flask, an aqueous potassium hydroxide solution (30 wt%, 5 mL) was added. Then, the mixture was evaporated in vacuo, and the distillate was trapped in the HCl solution. After removing the solvent from the HCl solution, the obtained residue and 1,3,5-trimethoxybenzene as an internal standard (16.9 mg, 100 μmol) were dissolved in DMSO-d_6. From the ^{1}H NMR spectrum illustrated in Figure S3a, the amounts of $^{15}NH_4Cl$ were determined to be 76 μmol (76% yield). ^{1}H NMR (DMSO-d_6): δ 7.20 (d, J = 72.0 Hz). The control experiments using **1a** instead of **^{15}N-1a** afforded 76 μmol of $^{14}NH_4Cl$ (76 [equiv./Mo]), which was confirmed by the triplet signal (^{1}H NMR (DMSO-d_6): δ 7.30 (t, J = 51.0 Hz)) in the ^{1}H NMR spectrum (Figure S3b).

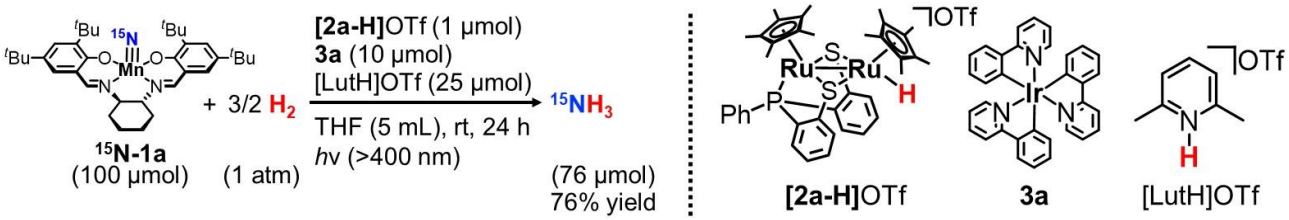

(a) With **1a-^{15}N**

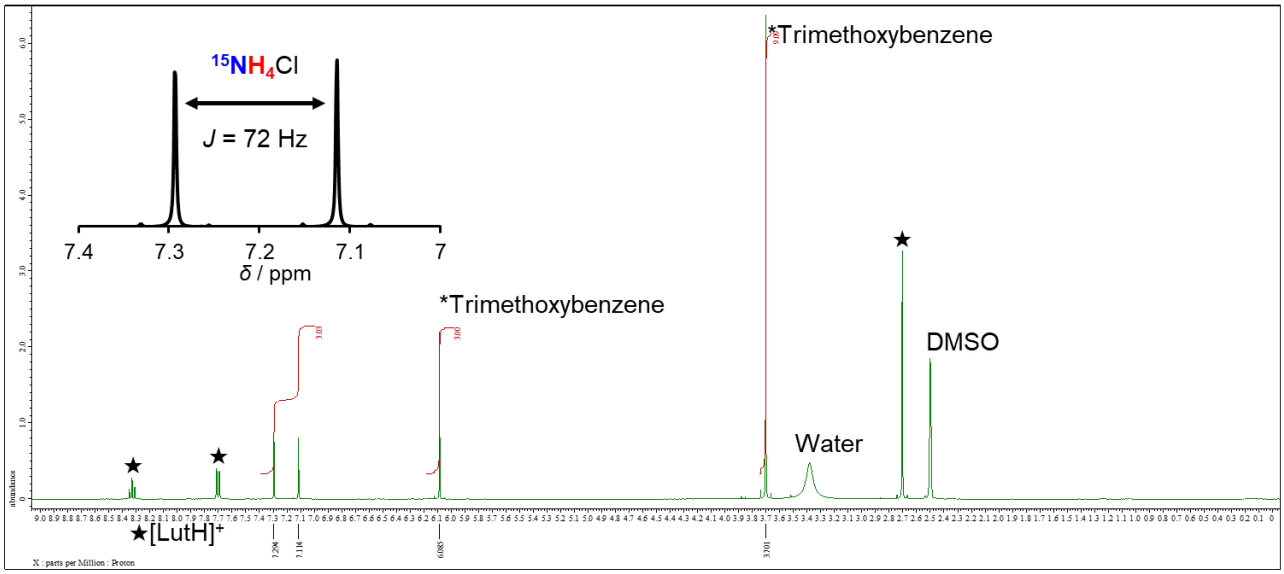

(b) With **1a**

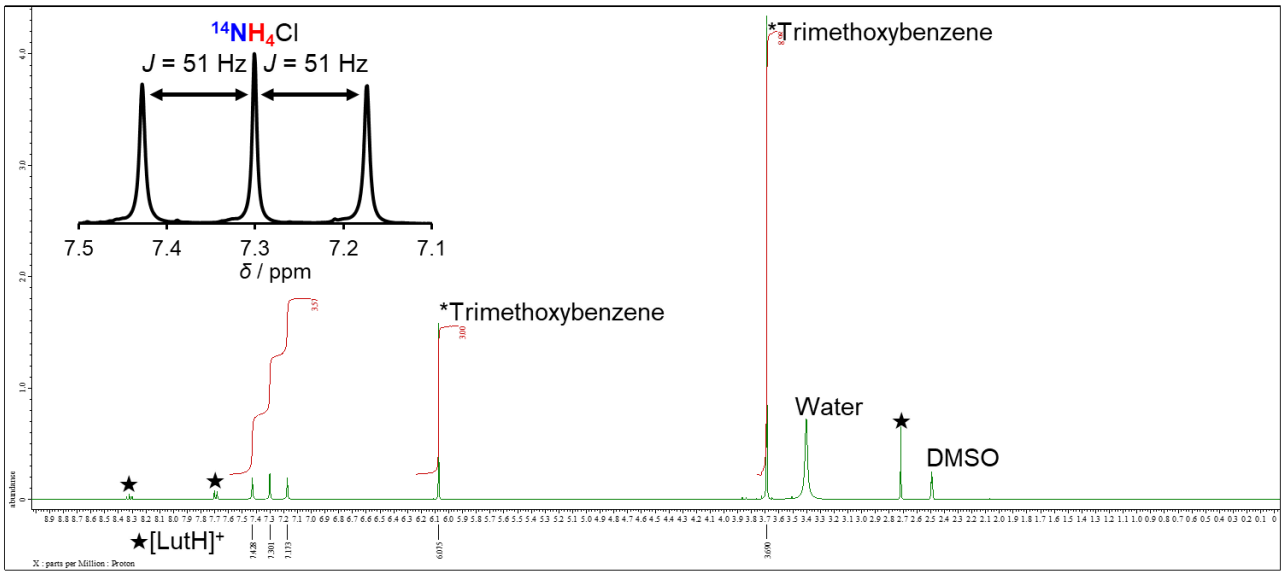

Figure S3. (a) ^{1}H NMR spectrum measured after the photocatalytic hydrogenation of **^{15}N-1a** in DMSO-d_6 containing 1,3,5-trimethoxybenzene as an internal standard. The spectrum of the control experiment conducted using **1a** instead of **^{15}N-1a** is shown in (b).

2.7. Isolation of dimanganese complex from reaction solution after photocatalysis

After photo-irradiation to a THF solution (5 mL) containing **1a** (61.4 mg, 100 µmol), **[2a-H]**OTf (1.0 mg, 1.0 µmol), **3a** (6.6 mg, 10 µmol), and [LutH]OTf (6.5 mg, 25 µmol) for 24 h as described in the general procedures (Section 2.1 in the Supporting Information), the solvent was removed under reduced pressure. Complex **4** was extracted with hexane from the obtained residue, and the insoluble materials, including **[2a-H]**OTf, **3a**, and [LutH]OTf, were filtered off with Celite. The solvent of the filtrate was removed under reduced pressure to yield complex **4** as orange solids. Yield: 55.9 mg, 93%. ^{1}H NMR (400 MHz, CD_2Cl_2): δ 13.70 (s, 2H), 8.30 (s, 2H), 7.29 (*br*, 2H), 6.99 (*br*, 2H), 3.70-3.67 (m, 4H), 3.36-3.32 (m, 2H), 2.46-1.50 (m, 54H), 1.38 (s, 18H), 1.21 (s, 18H). Elemental Anal. Calcd. (%) for $C_{72}H_{104}Mn_2N_4O_4$: C 72.09, H 8.74, N 4.67; Found (%): C 71.78, H 8.63, N 4.51. Slow evaporation of a concentrated hexane solution of complex **4** yielded needle-orange crystals suitable for X-ray analysis (Section 3 in the Supporting Information).

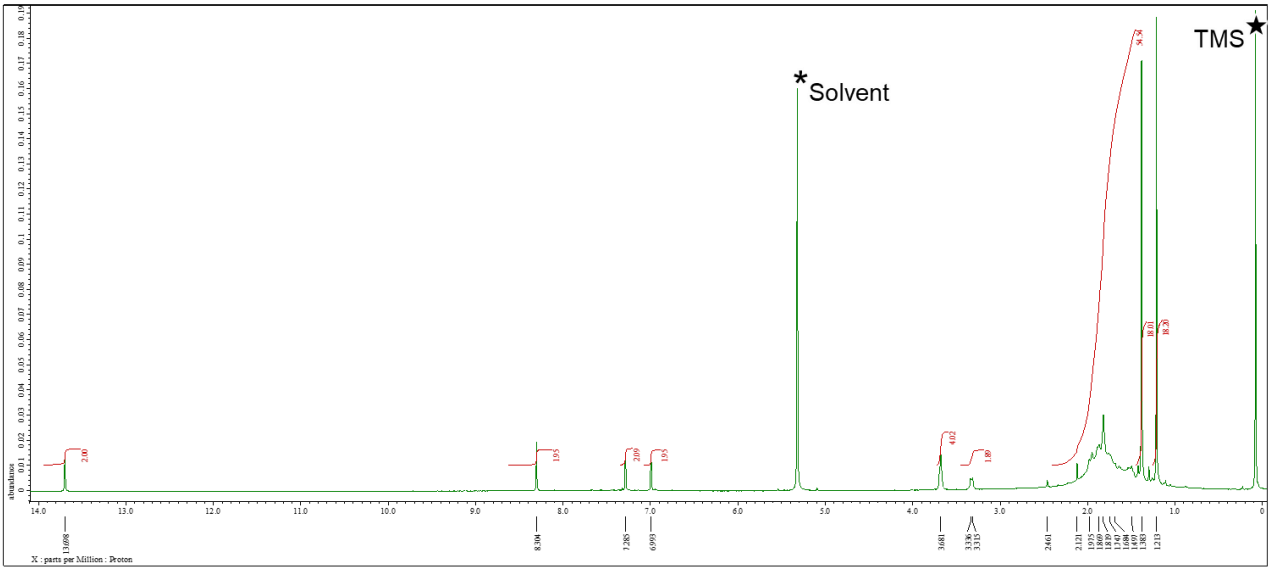

Figure S4. ^{1}H NMR spectrum of isolated complex **4** in CD_2Cl_2.

2.8. Analysis of reaction solution after photocatalysis

After photo-irradiation to a THF solution (5 mL) containing **1a** (61.4 mg, 100 μmol), **[2a-H]**OTf (1.0 mg, 1.0 μmol), **3a** (6.6 mg, 10 μmol), and [LutH]OTf (6.5 mg, 25 μmol) for 24 h as described in Section 2.1 in the Supporting Information, the resulting THF solution was transferred to an ESR tube in a glove box. The Electron Spin Resonance (ESR) spectrum (X-band) at room temperature was recorded on a Bruker Magnettech ESR5000 spectrometer (9.45 GHz) (Figure S5a). The spectra were simulated by EasySpin toolbox[14] on MATLAB. At the same time, the UV-vis absorption spectrum of the THF solution was recorded on a Shimadzu 2600-i (Figure S5b). In the obtained ESR spectrum, weak but characteristic signals at $g = 2.02$, with 6 lines, were observed. This should be reasonable because the total spin quantum number of Mn^{II} species is $I = 5/2$ (see Section 2.10 in the Supporting Information).[15] The fitting of the UV-vis absorption spectrum suggested that the solution mainly contained **[2a-H]**OTf, **3a**, and **4**.

After extracting complex **4** as described in Section 2.7 in the Supporting Information, the residual solids were analyzed by ^{1}H NMR spectroscopy using 1,3,5-trimethoxybenzene (11.4 mg, 67.8 μmol) as an internal standard in CD_2Cl_2 (Figure S6). In the spectrum, signals derived from both **[2a-H]**OTf and **3a** were observed. From the area ratios, the amount of **[2a-H]**OTf and **3a** were estimated to be 1.03 μmol and 10.2 μmol, respectively.

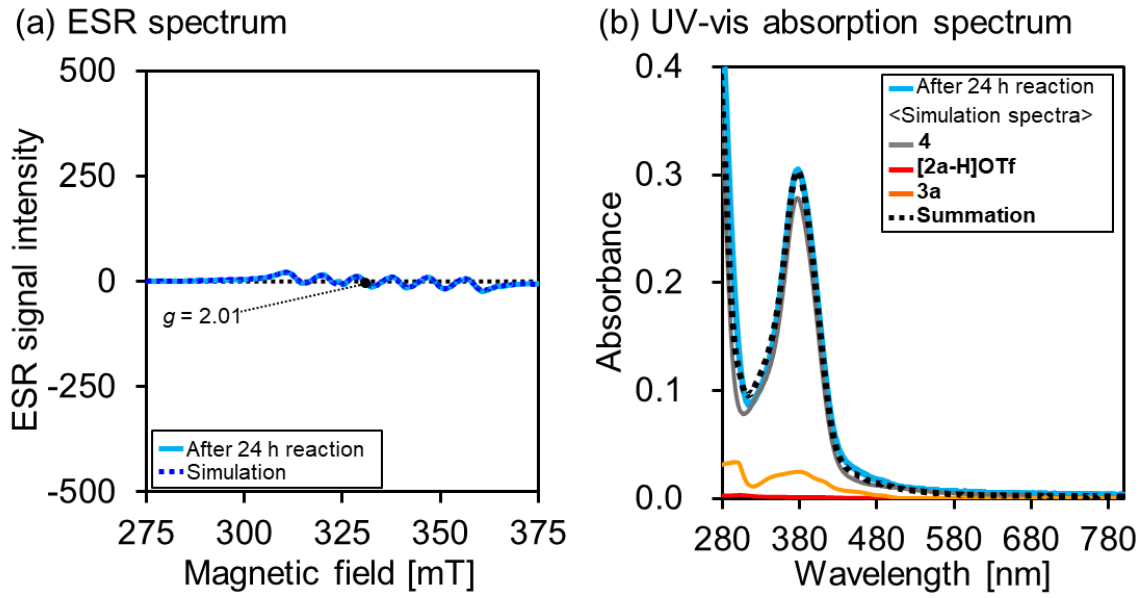

Figure S5. (a) ESR and (b) UV-vis absorption spectra of the reaction solution after 24-h photocatalytic reaction described in Section 2.1 in the Supporting Information. The simulated ESR spectrum (blue dotted line) is also illustrated in (a) (g value: 2.01, hyperfine constant A value: 255 MHz). The UV-vis absorption spectrum was measured after diluting the reaction solution to 100 times its original volume using an optical cell with a 1 mm path length. The black dotted line in (b) is the spectrum simulated from the summation of those of **[2a-H]**OTf (red, 2 μM), **3a** (orange, 20 μM), and **4** (gray, 100 μM).

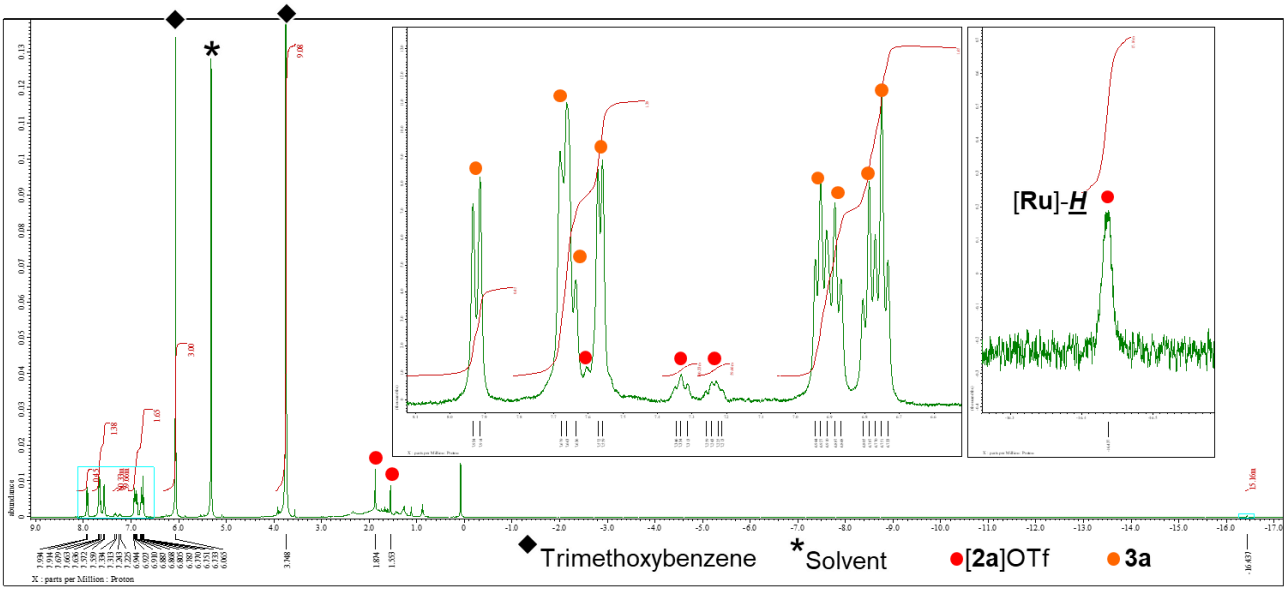

Figure S6. ^{1}H NMR spectrum of the residue obtained from the reaction solution for the hydrogenation of **1a** after extracting complex **4**. The solvent was CD_2Cl_2. 1,3,5-Trimethoxybenzene was added as an internal standard (11.4 mg, 67.8 μmol).

2.9. Reproduction of 1a from 4 obtained after the photocatalytic reactions

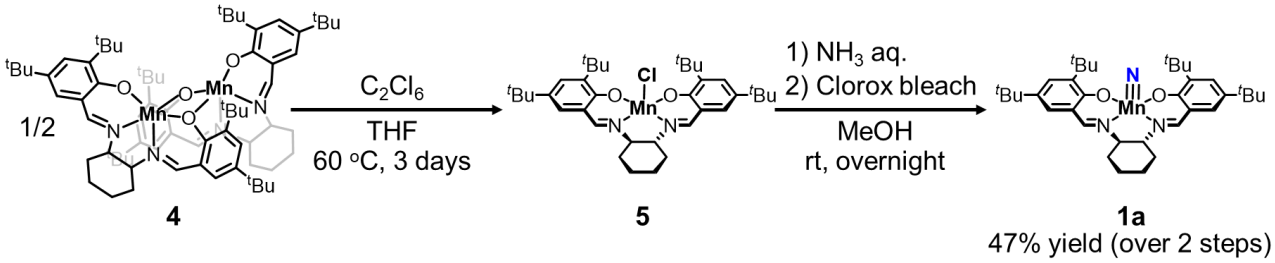

To reveal the reactivity of complex **4**, complex **1a** was reproduced from complex **4** by using the synthetic method[16] reported by Chirik, Knowles, and coworkers with several modifications as follows.

Complex **4** (56 mg, 47 μmol) and C_2Cl_6 (50 mg, 210 μmol) were dissolved in THF (5 mL). The resulting solution was heated at 60 ºC for 3 days. After cooling to room temperature, the solvent was removed under reduced pressure. The obtained residue was dissolved in CH_2Cl_2 (100 mL), and the UV-vis absorption spectrum was measured using a quartz cell (1 cm × 1 cm). As shown in Figure S7, the observed absorption spectrum was well-matched with that of the corresponding chloride complex **5** purchased from Tokyo Chemical Industry Co., Ltd., confirming that complex **5** was obtained with high selectivity. The product solution was evaporated under reduced pressure for the following further transformation. The obtained residue was dissolved in MeOH (2 mL), and ammonium hydroxide (ca. 6 M in water, 10 mL, 60 mmol) was then added dropwise to the solution over 5 min. The solution was stirred at room temperature for 0.5 h. To the vigorously stirring mixture, Chlorox Bleach (ca. 0.7 M NaOCl aq., 10 mL, 7 mmol) was added dropwise over 40 min. The resulting mixture was stirred at room temperature overnight. The precipitate was collected by filtration with Celite and was washed with MeOH. The solid on the Celite was dissolved in CH_2Cl_2, and the solvent of the filtrate was removed under reduced pressure. The obtained solid was purified by silica gel column chromatography (eluent: CH_2Cl_2). After removing the solvent under vacuum, the nitride complex **1a** was obtained as green solids. Yield: 28 mg, 48% over 2 steps. ^{1}H NMR (400 MHz, CD_2Cl_2): δ 7.99 (s, 1H), 7.93 (s, 1H), 7.48 (d, J = 2.8 Hz, 1H), 7.45 (d, J = 2.8 Hz, 1H), 7.00 (d, J = 2.2 Hz, 1H), 6.94 (d, J = 2.2 Hz, 1H), 3.46-3.42 (m, 1H), 3.03-2.98 (m, 1H), 2.68-2.66 (m, 1H), 2.53-2.50 (m, 1H), 2.02-2.01 (m, 2H), 1.61-1.59 (m, 1H), 1.50 (s, 9H), 1.45 (m, 9H), 1.42-1.38 (m, 3H), 1.29 (s, 9H), 1.28 (s, 9H). The ^{1}H NMR spectrum of the product was well-matched with the reported one[17] (Figure S8).

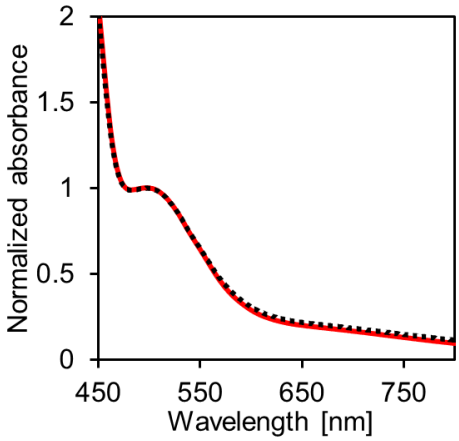

Figure S7. The UV-vis absorption spectrum of the product obtained from the oxidative chlorination of complex **4** (red solid line). The spectrum of the chloride complex **5**, purchased from Tokyo Chemical Industry Co., Ltd., is shown as the black dotted line. Both spectra were measured in THF and normalized at 500 nm.

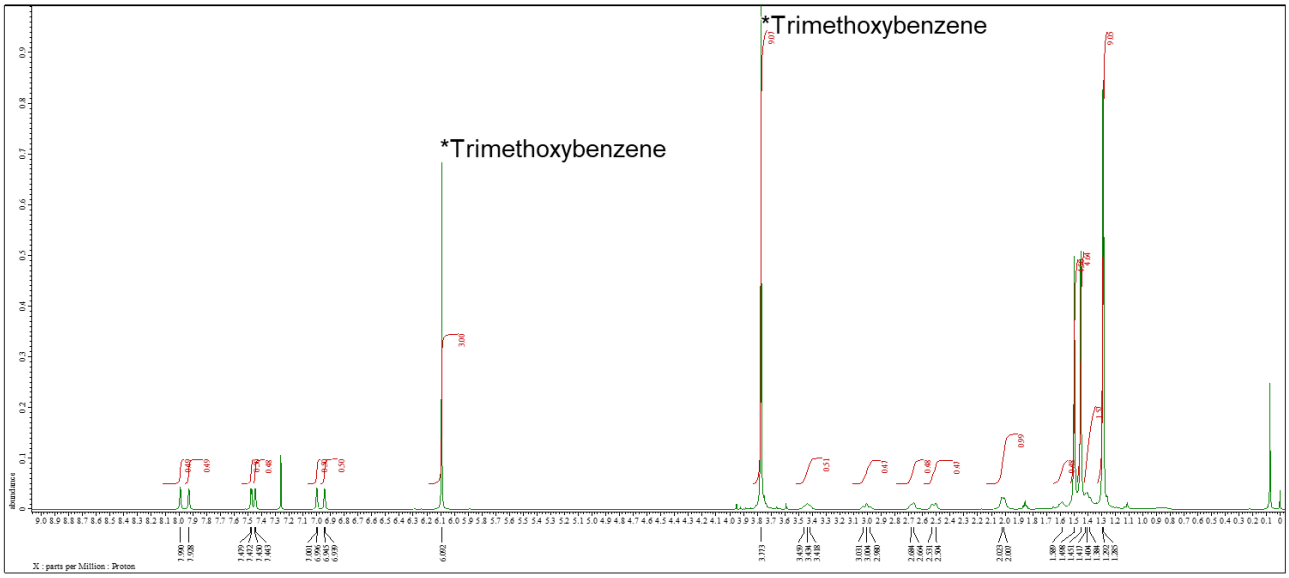

Figure S8. ^{1}H NMR spectrum of complex **1a** regenerated from complex **5**. The solvent was $CDCl_3$. The NMR yield (44.4 μmol, 48%) determined using 1,3,5-trimethoxybenzene as an internal standard (15.1 mg, 90.0 μmol) was coincident with the yield described above.

2.10. Investigation on interaction between complex 4 and [LutH]OTf

The ESR spectrum (X-band) of complex **4** (10 mM, Figure S9a, blue line) was recorded on a Bruker Magnettech ESR5000 spectrometer (9.45 GHz). The spectra were simulated by EasySpin toolbox[14] on MATLAB. In the obtained spectrum, no signal was observed, suggesting that complex **4** is an antiferromagnetically coupled dimer. When adding [LutH]OTf to the solution, a strong and characteristic signal at $g = 2.01$ containing 6 lines was observed. This should be reasonable because the total spin quantum number of the Mn^{II} species is $I = 5/2$.[15] The UV-vis absorption spectrum of complex **4** also changed drastically by adding [LutH]OTf (Figure S10a). These spectral changes almost ceased when adding more than 2 equiv. of [LutH]OTf. From these results, the molecular structure of complex **4** is changed in the presence of [LutH]OTf. Interestingly, when adding Lut instead of [LutH]OTf, both ESR and UV-vis absorption spectra were hardly changed (Figures S9b and S10b), suggesting that the aforementioned structural changes included the protonation of complex **4**. We also measured the ESR spectrum of the 2-methyltetrahydrofuran solution containing complex **4** and [LutH]OTf at 77 K. As illustrated in Figure S9c, it appears to exhibit hyperfine structure, possibly arising from the nitrogen atoms in the salen ligand, although simulating the spectrum was challenging because it may involve a few species. The significant broadening of the signal at room temperature may possibly be derived from the fluxional structure of the unidentified species (e.g., rapid protonation and deprotonation, rapid dimerization and dissociation, and/or rapid ligand substitution with the surrounding solvent molecules and OTf anions).

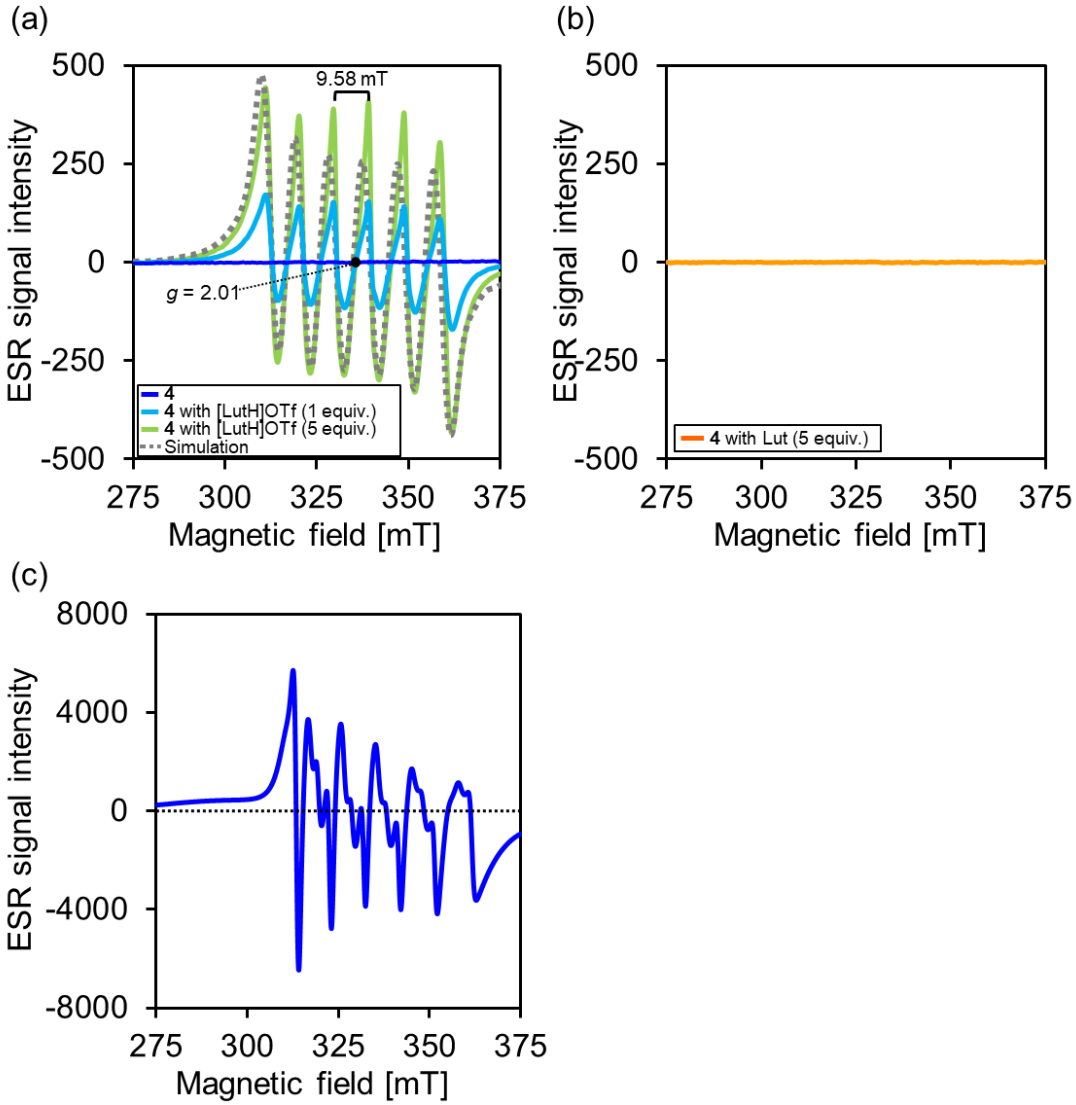

Figure S9. (a) The ESR spectrum of complex **4** (10 mM, blue) and those in the presence of 10 mM (sky blue) or 50 mM (yellow green) of [LutH]OTf in THF at rt. The simulated ESR spectrum (gray dotted line) is also illustrated in (a) (*g* value: 2.01, hyperfine constant *A* value: 263 MHz). (b) The ESR spectrum of complex **4** (10 mM) in the presence of 50 mM of Lut (orange) in THF at rt. (c)The ESR spectrum of the mixture of complex **4** (10 mM) and [LutH]OTf (50 mM) in 2-methyltetrahydrofuran at 77 K.

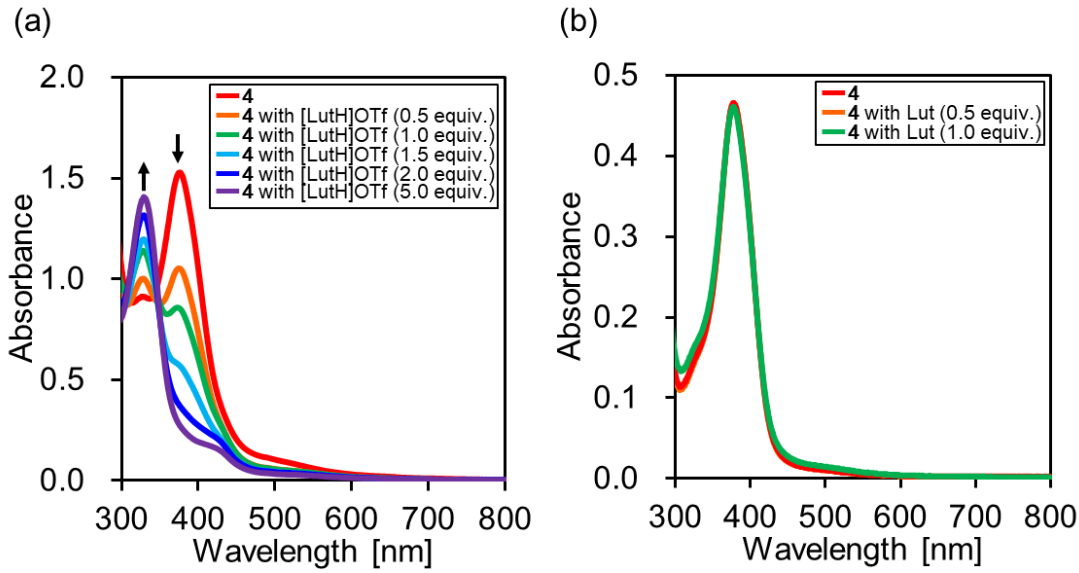

Figure S10. (a) UV-vis absorption spectrum of complex **4** (red line, 1 mM, path length: 1 mm) and those in the presence of 0.5 (orange), 1.0 (green), 1.5 (sky blue), 2.0 (blue), and 5.0 mM (purple) of [LutH]OTf in THF. (b) UV-vis absorption spectrum of complex **4** (red, 0.25 mM, path length: 1 mm) in the presence of 0.13 (orange) or 0.25 mM (green) of Lut in THF.

2.11. Photocatalytic ammonia formation under low partial pressure of dihydrogen

Table S9. Photocatalytic hydrogenation of **1a** in the presence of [**2a-H**]OTf, **3a**, and [LutH]OTf: photocatalysis under low partial pressure of dihydrogen.

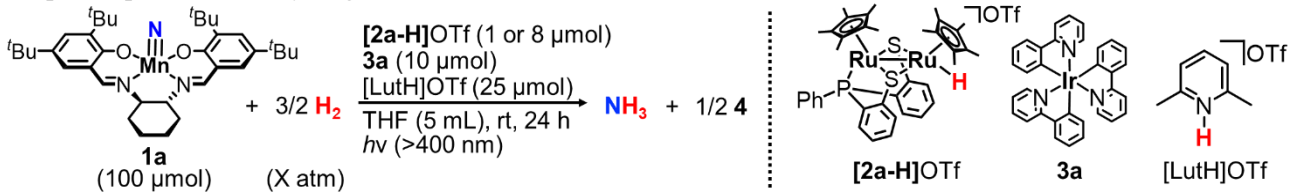

Entry	Partial pressure of H_2 [atm]	Amount of [**2a-H**]OTf [μmol]	NH_3 production [μmol][a,b]	NH_3 yield [%][b,c]
1-1	0.2	1	41.6	41.6
1-2	0.2	1	33.6	33.6
1-3	0.2	1	36.8 (31.2)	36.8 (31.2)
		(Average)	**37.3 ± 2.3**	**37.3 ± 2.3**
2-1	0.2	8	89.2 (85.9)	89.2 (85.9)
2-2	0.2	8	93.5 (89.4)	93.5 (89.4)
		(Average)	**91.3 ± 2.1**	**91.3 ± 2.1**
3-1	0.05	1	16.9	16.9
3-2	0.05	1	19.8	19.8
3-3	0.05	1	22.1 (18.0)	22.1 (18.0)
		(Average)	**19.6 ± 1.5**	**19.6 ± 1.5**
4-1	0.05	8	37.8	37.8
4-2	0.05	8	40.4 (38.1)	40.4 (38.1)
		(Average)	**39.1 ± 1.3**	**39.1 ± 1.3**

[a]The averages are shown with standard errors. [b]The values in the parentheses show the amount of detected free ammonia before addition of the KOH solution. [c]Yield based on **1a**.

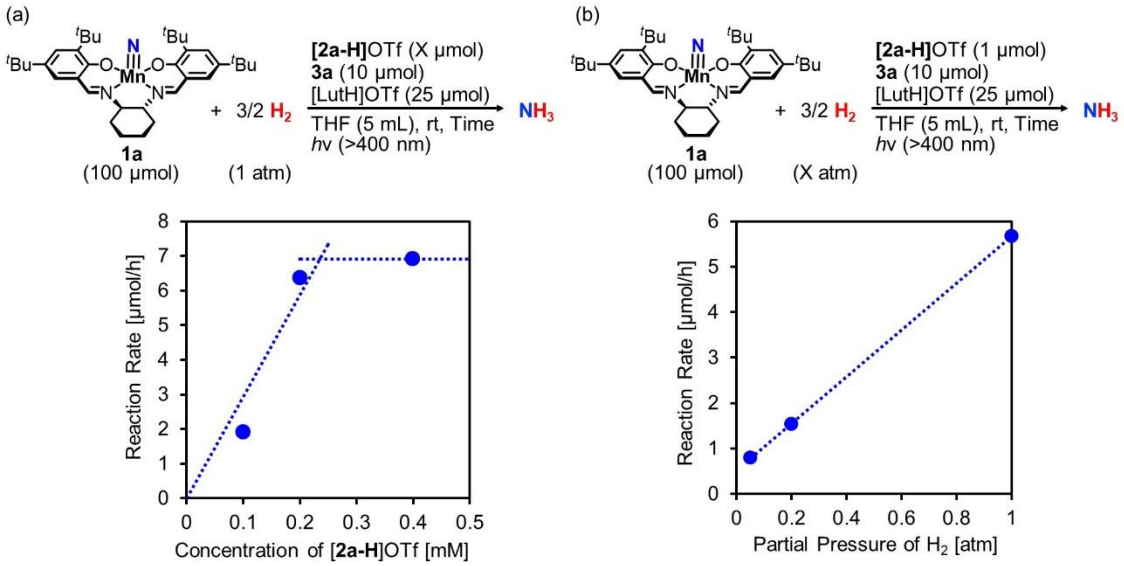

Figure S11. (a) Relationship between reaction rates for photocatalytic ammonia formation and the concentration of **[2a-H]**OTf in the presence of **1a** (100 μmol), **3a** (10 μmol), and [LutH]OTf (25 μmol) under 1 atm H_2. The reaction rates with 1 μmol (0.2 mM) or 0.5 μmol (0.1 mM) of **[2a-H]**OTf were calculated from the amount of ammonia shown in Table S1 (0.2 mM: 38 μmol after 6 h), or Table 1 in the manuscript (0.1 mM: 46 μmol after 24 h). The reaction rate with 2 μmol (0.4 mM) of **[2a-H]**OTf was calculated from the amount of ammonia produced after 6-h irradiation (41 μmol). (b) Relationship between reaction rates for photocatalytic ammonia formation and partial pressure of dihydrogen in the presence of **1a** (100 μmol), **[2a-H]**OTf (1.0 μmol), **3a** (10 μmol), and [LutH]OTf (25 μmol). The reaction rates were calculated from the amount of ammonia shown in Table S1 (1 atm: 16.9 μmol after 3 h) or Table S9 (0.2 atm: 37 μmol after 24 h, 0.05 atm: 19 μmol after 24 h).

3. X-ray crystallography

Diffraction data for **1c** and **4** were collected for the 2θ range of 4−62° for **1c** or 4−50° for **4** at −180 °C on a Rigaku XtaLAB Synergy-S diffractometer equipped with a HyPix-6000HE Hybrid Photon Counting (HPC) detector and VariMax optics using multilayer mirror monochromated Mo Kα (λ = 0.71073 Å) radiation. Intensity data were corrected for Lorentz and polarization effects and for empirical and numerical absorptions using the *CrysAlisPro* package,[18] while structure solutions and refinements were carried out by using the *CrystalStructure* crystallographic software package.[19] The positions of the non-hydrogen atoms were generally determined by direct methods (SHELXT Version 2014/5)[20] and subsequent Fourier syntheses (SHELXL Version 2016/6),[21] and were refined on F_o^2 using all unique reflections by full-matrix least-squares with anisotropic thermal parameters. Details of crystallographic data are summarized in Table S10. The carbon atoms of cyclohexyl moieties in **1c** and **4**, and the carbon atoms of the hexane molecule and one of the *tert*-butyl groups in **4**, were solved as disorders between two positions. It should be noted that the quality of the crystal was not high enough to obtain low R values due to the low stability and high air sensitivity of complex **4**. Therefore, a detailed discussion of the molecular structure of complex **4**, including its bond lengths and angles, was difficult. Although the R values were not high enough, we obtained the following important conclusions from the ORTEP drawing of complex **4**: the nitride ligands were successfully consumed by photocatalytic hydrogenation, and the residual manganese salen complexes will form an antiferromagnetically coupled dimer, resulting in no ESR signals.

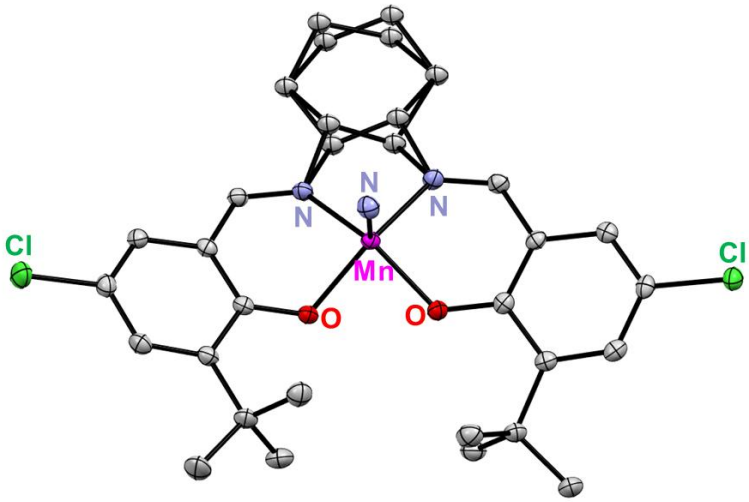

Figure S12. The ORTEP drawing of the resulting manganese complex **1c** obtained after the photocatalytic hydrogenation reaction. Thermal ellipsoids are shown at the 50% level. Hydrogen atoms are omitted for clarity. Gray, red, purple, green, and pink correspond to C, O, N, Cl, and Mn atoms, respectively.

Table S10. Crystallographic data of molybdenum complexes **1c** and **4** synthesized in this work.

	1c	**4•C_6H_{14}**
chemical formula	$C_{28}H_{34}Cl_2MnN_3O_2$	$C_{78}H_{118}Mn_2N_4O_4$
CCDC number	2413808	2413811
formula weight	570.44	1285.69
dimensions of crystals, mm^3	0.462 × 0.067 × 0.026	0.293 × 0.113 × 0.086
crystal color, habit	green, needle	orange, needle
crystal system	monoclinic	triclinic
space group	$P2_1/c$	P-1
a, Å	8.4062(2)	14.5819(6)
b, Å	25.5135(6)	15.3597(7)
c, Å	12.4658(3)	17.0815(6)
α, deg	90	78.090(3)
β, deg	93.782(2)	79.223(3)
γ, deg	90	86.702(3)
V, Å^3	2667.74(11)	3676.7(3)
Z	4	2
ρ_{calcd}, g cm^{-3}	1.420	1.161
F(000)	1192	1292
μ, cm^{-1}	7.257	3.926
temperature, °C	–180	–180
trans. factors range	0.611 – 0.981	0.635 – 0.967
no. reflections measured	30175	61627
no. unique reflections (R_{int})	7032 (0.0376)	18680 (0.0798)
no. parameters refined	335	763
R_1 ($I > 2\sigma(I)$)[a]	0.0346	0.1105
wR_2 (all data)[b]	0.0716	0.2617
GOF (all data)[c]	1.00	1.00
max diff peak / hole, e $Å^{-3}$	+0.74 / –0.43	+2.31 / –0.59

[a] $R_1 = \Sigma||F_o|-|F_c||/\Sigma|F_o|$.

[b] $wR_2 = [\Sigma w(F_o^2-F_c^2)^2/\Sigma w(F_o^2)^2]^{1/2}$, $w = 1/[\sigma^2(F_o^2) + (qP)^2 + rP]$, $P = (\mathrm{Max}(F_o^2, 0) + 2F_c^2)/3$

(**1c**: $q = 0$; $r = 3.078$, **4**·C_6H_{14}: $q = 0$, $r = 59.1$)

[c] GOF = $[\Sigma w(F_o^2-F_c^2)^2/(N_o-N_{params})]^{1/2}$

4. Photophysical and photochemical properties

4.1. General methods

Photophysical and photochemical properties were measured using a custom-ordered Pyrex optical cell connected with a ground-glass joint (optical path length: 1 cm or 0.1 cm). All solutions for measurement were prepared in a glovebox and added to the cell, which was sealed with a ground-glass stopper applied with vacuum grease (Figure S12). UV−vis absorption spectra of manganese nitride complexes, catalysts for dihydrogen oxidation, and photosensitizers were recorded on a Shimadzu 2600-i. Emission spectra of photosensitizers were recorded using Shimadzu RF-6000. The excitation energy ($E_{0\text{-}0}$) was determined by Franck-Condon analysis using spectral fitting of emission spectra based on the following equation:[23]

$$I(\tilde{\boldsymbol{\nu}}) = \sum_{n=0}^{10} \left(\frac{E_{0-0} - n\tilde{\nu}_{vib}}{E_0}\right)^3 \left(\frac{S^n}{n!}\right) exp\left[-4ln2\left(\frac{\tilde{\nu} - (E_{0-0} - n\tilde{\nu}_{vib})}{\tilde{\nu}_{1/2}}\right)\right] \quad \text{(S2)}$$

($\tilde{\boldsymbol{\nu}}$: wavenumbers of emission, $\boldsymbol{S}$: measures of the distortion in the acceptor modes of the complexes, $\tilde{\boldsymbol{\nu}}_{vib}$: the energies of acceptor modes, $\tilde{\boldsymbol{\nu}}_{1/2}$: the full width at half maximum of the 0-0 vibronic component in the emission spectra)

The emission decay curves of photosensitizers were measured using UNISOKU TSP-1000 with a pulsed YAG laser as an exciting light source (λ_{ex} = 355 nm, 200 mJ). The detection wavelength was 600 nm. The emission lifetimes (τ) were determined by fitting the emission decay curves with a single exponential function ($I(t) = A\exp(-t/\tau)$; I: emission intensity, A: pre-exponential factor). The Stern-Volmer analyses for the solutions of **3a** (25 μM) were performed using variable concentrations of quenchers (i.e., **1a**, [**2a-H**]OTf, and [LutH]OTf).

Figure S13. Photograph of the optical cell with a Clear Mating Plug for spectroscopic analysis.

4.2. Photophysical properties

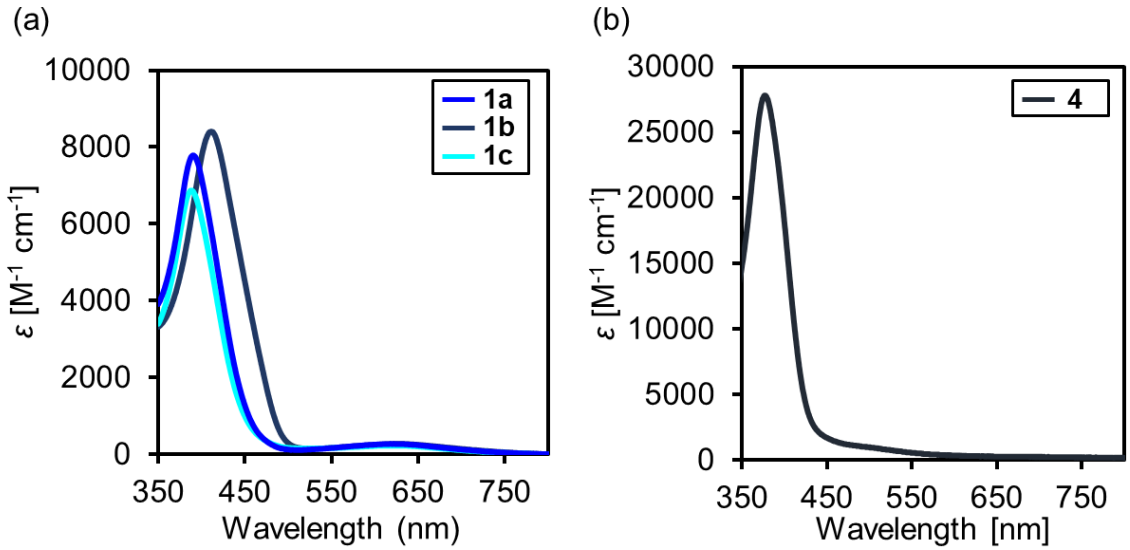

Figure S14. (a) UV-vis spectra of **1a** (blue), **1b** (navy), and **1c** (aqua blue) in THF. (b) UV-vis spectrum of **4** (gray) in THF.

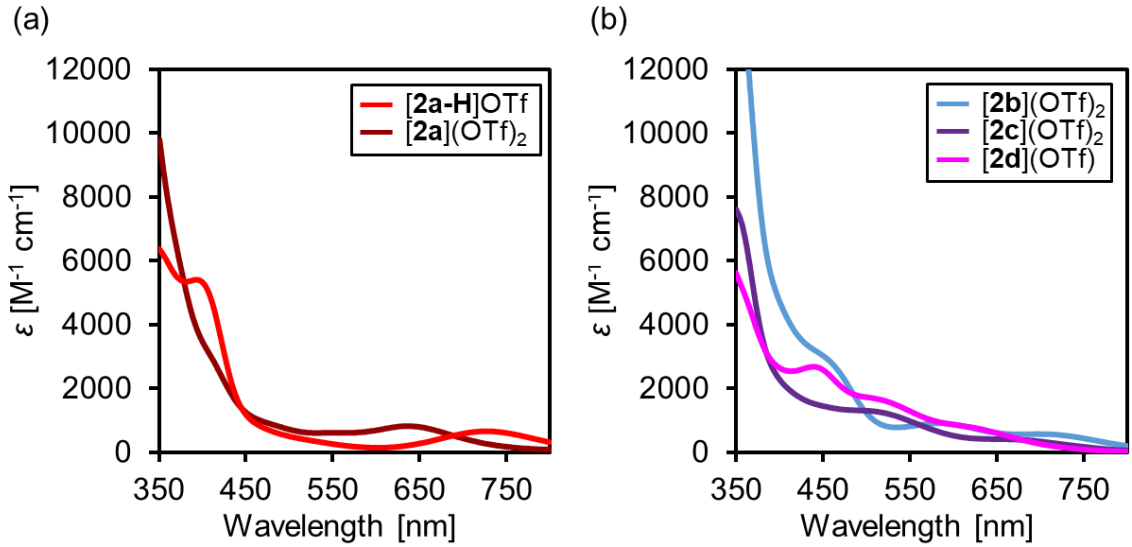

Figure S15. (a) UV-vis absorption spectra of [**2a-H**]OTf (red), [**2a**](OTf)$_2$ (dark red) in THF. (b) UV-vis absorption spectra of [**2b**](OTf)$_2$ (sky blue), [**2c**](OTf)$_2$ (violet), and [**2d**]OTf (pink) in THF.

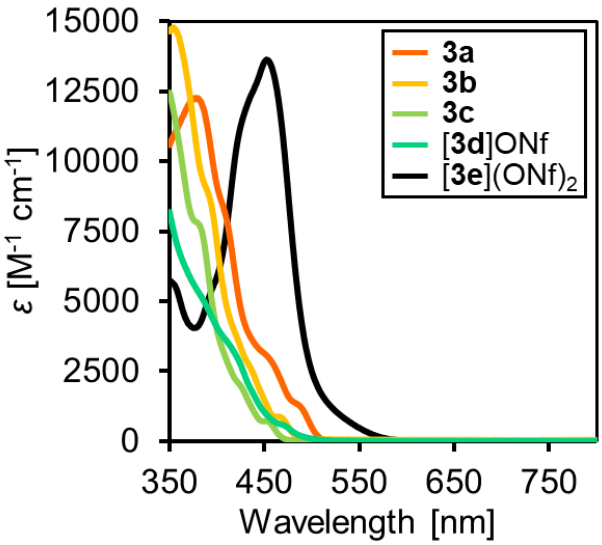

Figure S16. UV-vis spectra of **3a** (orange), **3b** (yellow), **3c** (yellow green), [**3d**]ONf (green), and [**3e**](ONf)$_2$ (black) in THF.

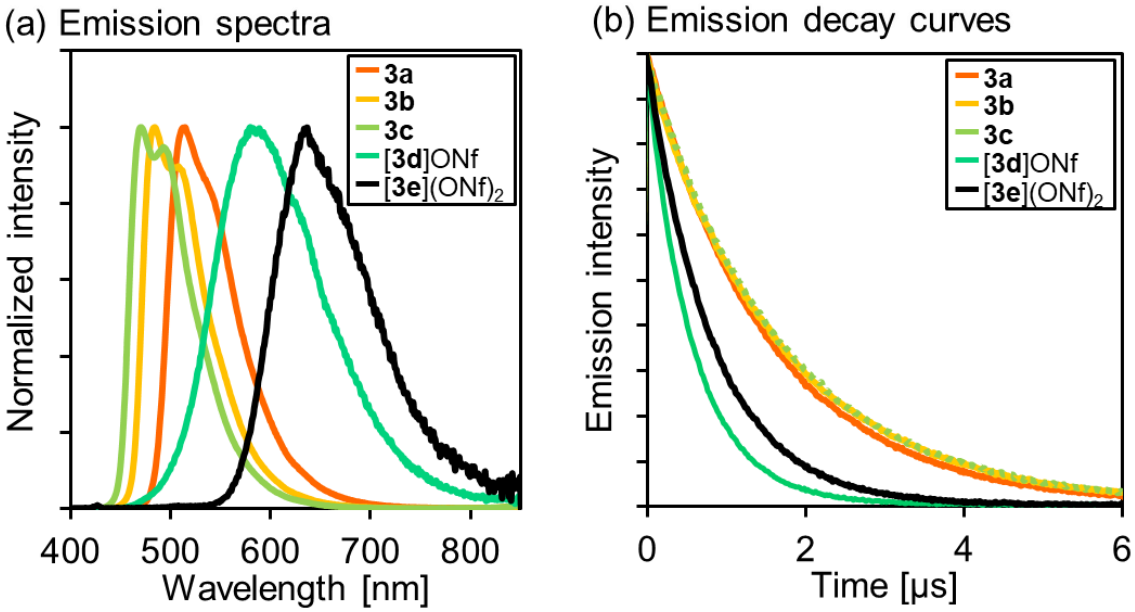

Figure S17. (a) Emission spectra and (b) emission decay curves of **3a** (orange), **3b** (yellow), **3c** (yellow green), [**3d**]ONf (green), and [**3e**](ONf)$_2$ (black) in THF (25 µM).

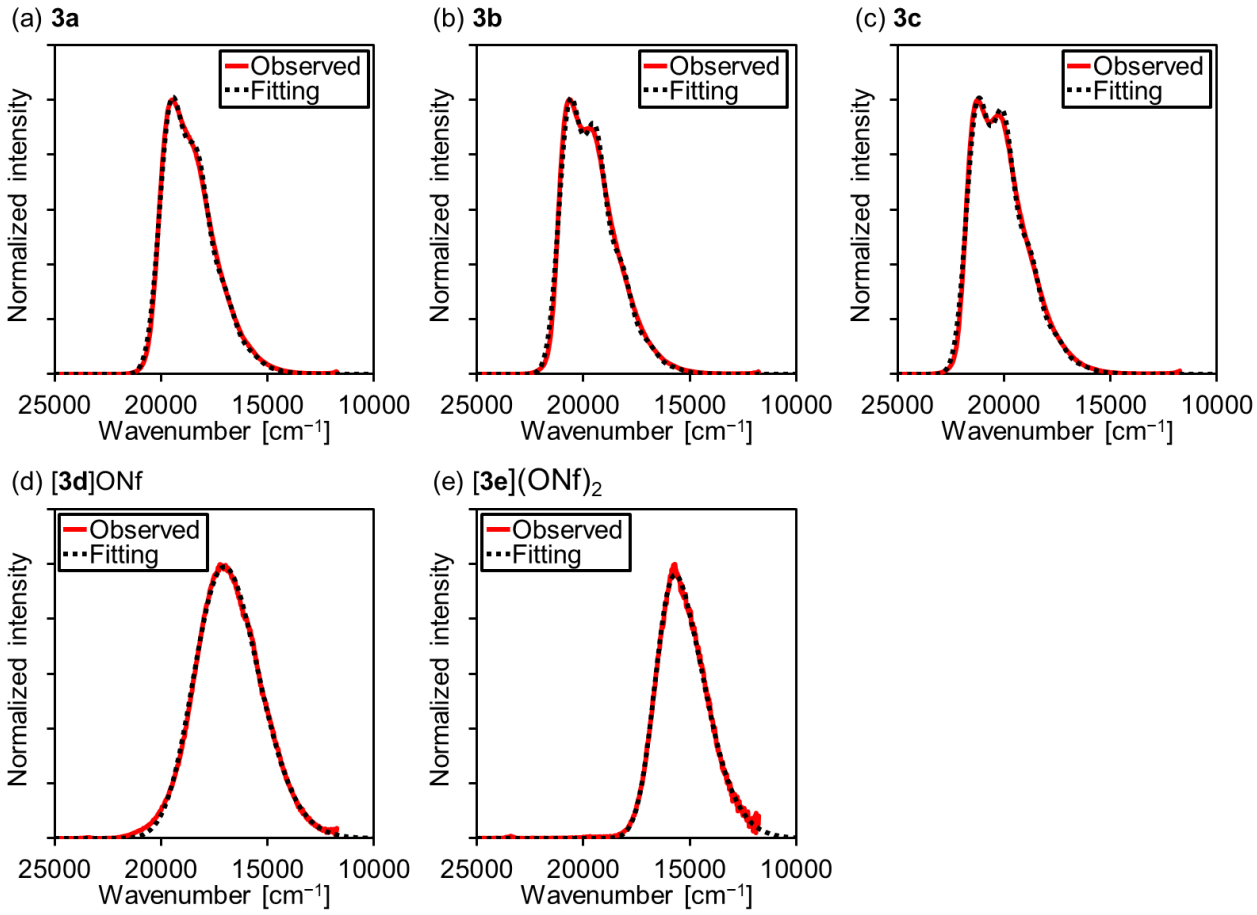

<Fitting parameters>

Photosensitizer	$E_{0\text{-}0}$ / cm^{-1}	$E_{0\text{-}0}$ / eV	$\tilde{\nu}_{vib}$ / cm^{-1}	S	$\tilde{\nu}_{1/2}$ / cm^{-1}
3a	19500	2.42	1230	0.932	1290
3b	20700	2.56	1210	1.05	1200
3c	21300	2.64	1220	1.11	1220
[3d]ONf	17900	2.22	1050	1.32	2610
[3e](ONf)$_2$	15940	1.98	1290	0.718	1840

Figure S18. Franck-Condon analysis of photosensitizers in THF (25 μM) using eqn S2.

Table S11. Photophysical properties of the photosensitizers.

Photosensitizer	λ_{em} [nm] [a]	$E_{0\text{-}0}$ [eV] [b]	τ [μs] [c]
3a	515	2.42	1.54
3b	485, 508	2.56	1.66
3c	471, 493	2.64	1.67
[3d]ONf	580	2.22	0.57
[3e]$(ONf)_2$	637	1.98	0.82

[a]Emission maximum wavelength (Figure S17a). [b]Excitation energy determined by Franck-Condon analysis (Figure S18). [c]Emission lifetimes determined from the fitting of emission decay curves (Figure S17b).

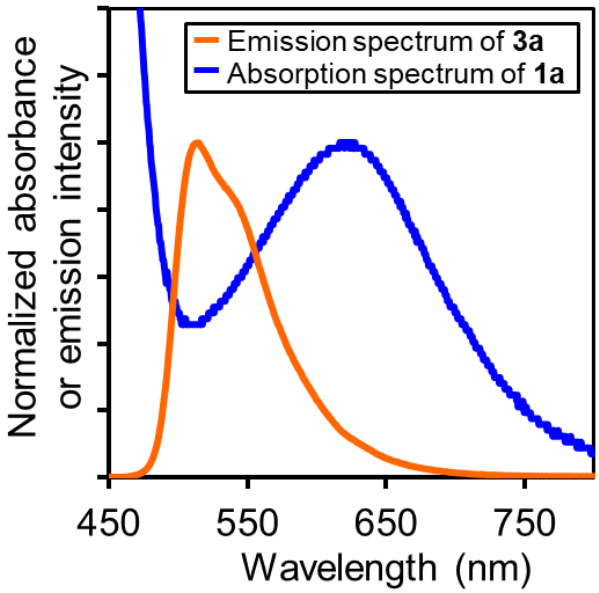

Figure S19. The overlap between the UV-vis spectrum of **1a** (blue) and the emission spectrum of **3a** (orange) in THF. The spectra were normalized at their absorption or emission band maxima.

4.3. Stern-Volmer analysis

Stern-Volmer luminescence quenching studies for the solutions of the photosensitizer **3a** (25 μM) with various concentrations of a quencher ([Q]) were performed under an Ar atmosphere using emission decay curves. The emission decay curves were monitored using UNISOKU TSP-1000 with a pulsed YAG laser as an exciting light source (λ_{ex} = 355 nm, 200 mJ). The detection wavelength was 600 nm. To determine the emission lifetimes (τ), the emission decay curves were fitted using a single exponential function ($I(t) = A\exp(-t/\tau)$; I: emission intensity, A: pre-exponential factor). By comparing the emission lifetime in the absence of any quencher (τ_0), the Stern-Volmer analyses were performed based on the following equation:

$$\tau_0/\tau = 1 + K_{SV}[Q] = k_Q\tau_0[Q] \qquad \text{(S3)}$$

where K_{SV} [M^{-1}]: Stern-Volmer constant, k_Q [$M^{-1}s^{-1}$]: Quenching rate constant for emission from **3a** by the Quencher. The emission decay curves and each emission lifetime are summarized in Figure S21 and Table S13. For the Stern-Volmer analysis in the presence of Quenchers 1 and 2, we used eqn. S6 for the fitting, which was derived from eqns. S4 and S5.

The emission quantum yield in the presence of Quencher 1 (Φ_0)

$$\Phi_0 = \frac{k_r}{k_r+k_{nr}+k_{Q1}[Q1]} \qquad \text{(S4)}$$

(k_r [s^{-1}]: Rate constants for radiative deactivation, k_{nr} [s^{-1}]: Rate constants for non-radiative deactivation, k_{Q1} [$M^{-1}s^{-1}$]: Quenching rate constant for emission from **3a** by Quencher 1, [Q1] [M]: Concentration of Quencher 1.)

The emission quantum yield in the presence of Quenchers 1 and 2 (Φ)

$$\Phi = \frac{k_r}{k_r+k_{nr}+k_{Q1}[Q1]+k_{Q2}[Q2]+k_{Q1Q2}[Q1][Q2]} \qquad \text{(S5)}$$

(k_{Q2} [$M^{-1}s^{-1}$]: Quenching rate constant for emission from **3a** by Quencher 2; [Q2] [M]: Concentration of Quencher 2; k_{Q1Q2} [$M^{-2}s^{-1}$]: Quenching rate constant for emission from **3a** by the reaction among **3a***, Quencher 1, and Quencher 2)

The Stern-Volmer equation emission quantum yield in the presence of Quenchers 1 and 2

$$\Phi_0/\Phi = \tau_0/\tau = 1 + \frac{k_{Q2}+k_{Q1Q2}[Q1]}{k_r+k_{nr}+k_{Q1}[Q1]}[Q2] \qquad \text{(S6)}$$

The efficiencies of the emission quenching by a quencher ($\eta_q(Qn)$, n = 1-3) in the reaction solution (Table 3 in the manuscript) were estimated using the Stern-Volmer constants $K_{SV}(Qn)$ (i.e., the slopes of the Stern-Volmer plots) and the concentration of the quencher ([Qn]) based on the following equation:

$$\eta_q(Qn) = K_{SV}(Qn)\times[Qn] / \{1 + K_{SV}(Q1)\times[Q1] + K_{SV}(Q2)\times[Q2] + K_{SV}(Q3)\times[Q3]\} \qquad \text{(S7)}$$

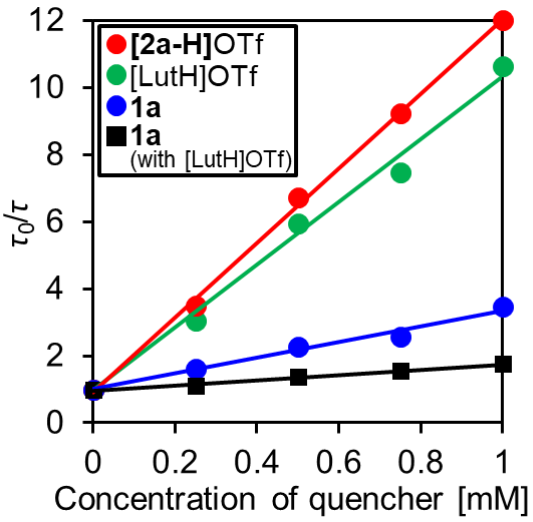

Figure S20. Stern-Volmer luminescence quenching studies of **3a** with **1a** (blue), [**2a-H**]OTf (red), or [LutH]OTf (green). The black line is the Stern-Volmer plots using various concentrations of **1a** (0-1 mM) in the presence of [LutH]OTf (0.25 mM).

Table S12. Emission lifetimes of **3a** in the presence of various concentrations of **1a**, [**2a-H**]OTf, [LutH]OTf.[a]

Quencher	K_{SV} [mM^{-1}][a]	k_Q [$M^{-1}s^{-1}$][b]	η_q [%][c]
1a	2.4	1.6×10^9	49
[2a-H]OTf	11	7.6×10^9	2
[LutH]OTf	9.3	6.4×10^9	48
1a in the presence of [LutH]OTf (0.25 mM)	0.78	6.6×10^{11} [d]	–

[a]The Stern-Volmer constants determined from the slope of the fitting curves illustrated in Figure 5 of the manuscript. [b]The quenching rate constants determined from K_{SV} and the emission lifetime of **3a** in the absence of any quencher (τ_0, $K_{SV} = k_Q\tau_0$). [c]The quenching fractions in the reaction solution calculated based on eqn. S7 in the Supporting Information. [d]The quenching rate constant derived from the reaction among **3a***, **1a**, and [LutH]OTf was determined based on eqn. S6 in the Supporting Information.

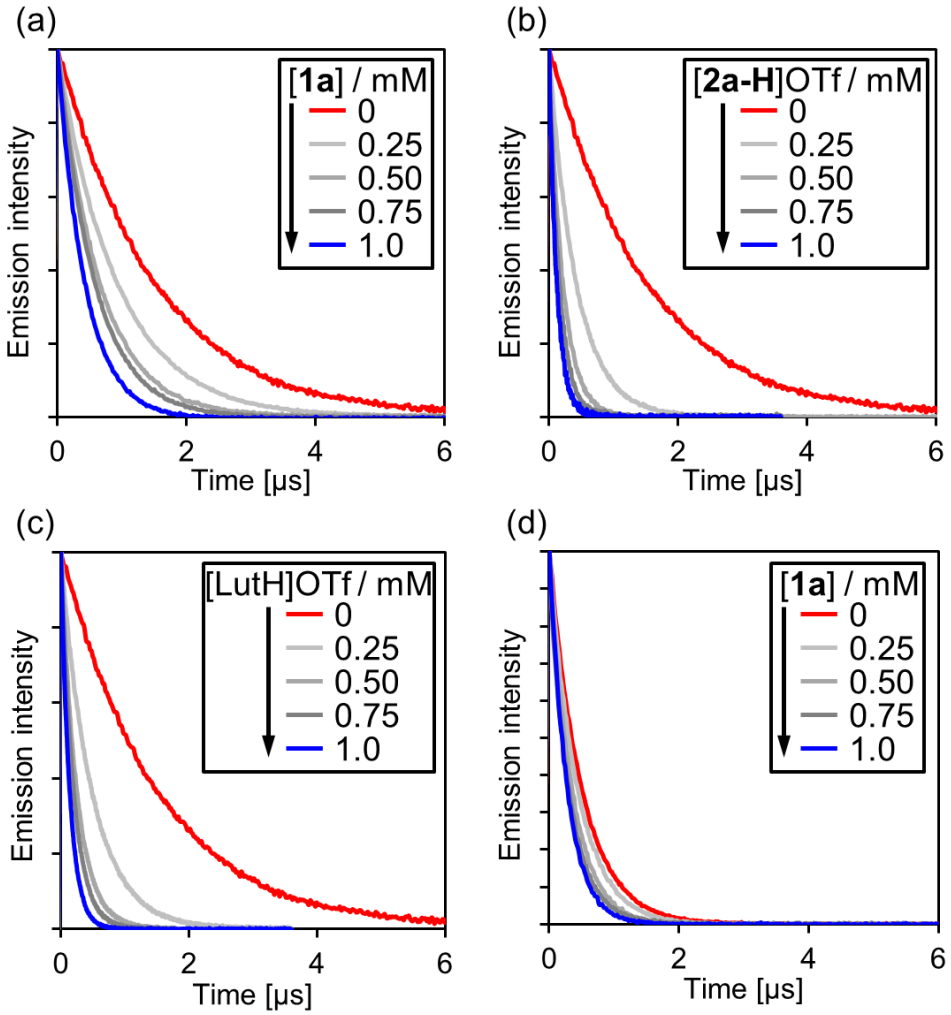

Figure S21. Emission decay curves of **3a** in the presence of various concentrations ([Q] = 0-1 mM) of (a) **1a**, (b) [**2a-H**]OTf, or (c) [LutH]OTf. In the case of (d), the concentration of **1a** was changed from 0 to 1 mM in the presence of [LutH]OTf (0.25 mM). The solvent was THF. The excitation and detection wavelengths were 355 and 600 nm, respectively.

Table S13. Emission lifetimes of **3a** in the presence of various concentrations of **1a**, [**2a-H**]OTf, [LutH]OTf.[a]

Concentration of Quencher [mM]	**1a**	[**2a-H**]OTf	[LutH]OTf	**1a** (in the presence of [LutH]OTf (0.25 mM))[b]
0	1.46	1.46	1.46	0.48
0.25	0.91	0.42	0.48	0.43
0.50	0.64	0.22	0.25	0.35
0.75	0.57	0.18	0.20	0.31
1.0	0.42	0.12	0.14	0.27

[a]The emission lifetimes were determined from the slopes of the fitting curve illustrated in Figure S21. The Stern-Volmer plots using values in this table are shown in Figure S20. [b]The concentration of **1a** was changed from 0 to 1.0 mM in the presence of [LutH]OTf (0.25 mM).

5. Cyclic voltammetry

5.1. General procedures

Cyclic voltammograms of the photosensitizers and tertiary phosphines were recorded on an electrochemical analyzer (ALS 1200, BAS Inc.) with glassy carbon disk (diameter: 3 mm) as a working electrode and Pt wire as a counter electrode in THF containing 1 mM of sample and 0.1 M of [^{n}Bu$_4$N][PF$_6$] (TBAPF$_6$) as a supporting electrolyte at a scan rate of 0.1 V/s at room temperature under N_2 atmosphere. All potentials were measured against an $Ag^{0/+}$ electrode and converted to the values *vs*. ferrocene/ferrocenium ($Fc^{0/+}$) referenced to an external standard ($Fc^{0/+}$). Cyclic voltammograms are shown in Figures S22-29 and Tables S14-17.

5.2. Cyclic voltammogram

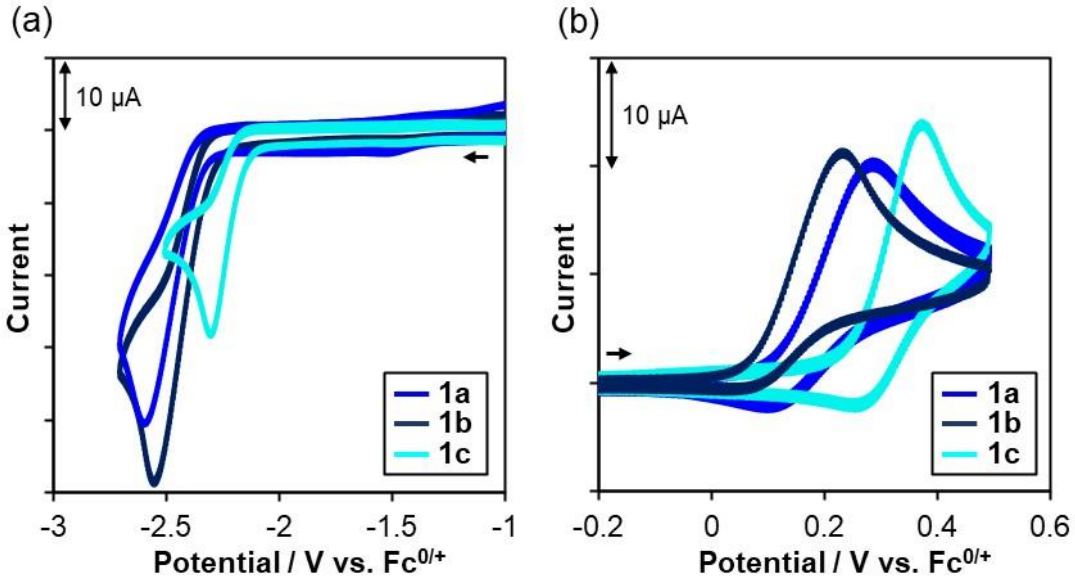

Figure S22 Cyclic voltammograms at (a) the first reduction waves and (b) the first oxidation waves of **1a** (blue), **1b** (navy), and **1c** (aqua blue) in a THF solution containing TBAPF$_6$ (0.1 M) as a supporting electrolyte at a sweep rate of 100 mV s^{-1} under N_2. A glassy carbon electrode (diameter: 3 mm) and a Pt wire were used as working and counter electrodes, respectively. All potentials were measured against an $Ag^{0/+}$ electrode and converted to the values *vs*. ferrocene/ferrocenium ($Fc^{0/+}$) referenced to an external standard ($Fc^{0/+}$). The scan was started (a) from −0.4 V to the negative direction or (b) from −0.4 V to the positive direction.

Table S14. Electrochemical properties of the manganese nitride complexes in THF. [a]

Mn Complex	E_{red} [V] [b]	E_{ox} [V] [b]
1a	−2.60	+0.26
1b	−2.55	+0.23
1c	−2.30	+0.37

[a]Measured in a THF solution containing the complex (0.5 mM) and TBAPF$_6$ (0.1 M) with a scan rate of 100 mV s^{-1} under a N_2 atmosphere (Figure S22. [b]Peak potentials (E_p) vs. $Fc^{0/+}$.

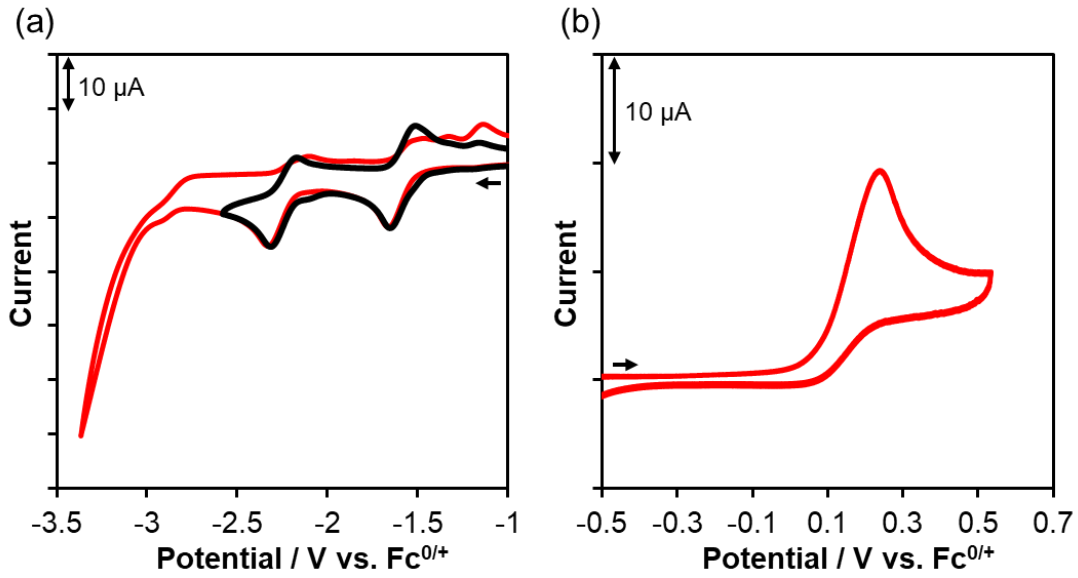

Figure S23 (a) The reduction waves and (b) the oxidation waves in cyclic voltammograms of [**2a-H**]OTf in a THF solution containing $TBAPF_6$ (0.1 M) as a supporting electrolyte at a sweep rate of 100 mV s^{-1} under N_2. A glassy carbon electrode (diameter: 3 mm) and a Pt wire were used as working and counter electrodes, respectively. All potentials were measured against an $Ag^{0/+}$ electrode and converted to the values *vs*. ferrocene/ferrocenium ($Fc^{0/+}$) referenced to an external standard ($Fc^{0/+}$). The scan was started (a) from −0.6 V to the negative direction or (b) from −0.6 V to the positive direction.

The voltammogram shown in (a) contained two reversible waves at −1.58 and −2.24 V, meaning that [**2a-H**]OTf can accept electrons from **3a*** (E_{ox}*: −2.15 V) to result in promoting the charge recombination processes. An irreversible oxidation wave was observed at +0.24 V in (b), meaning that the one-electron-oxidized species of **3a** (**3a**$^+$, E_{ox}: +0.27 V) can oxidize [**2a-H**]OTf to trigger the catalytic cycle for dihydrogen oxidation.

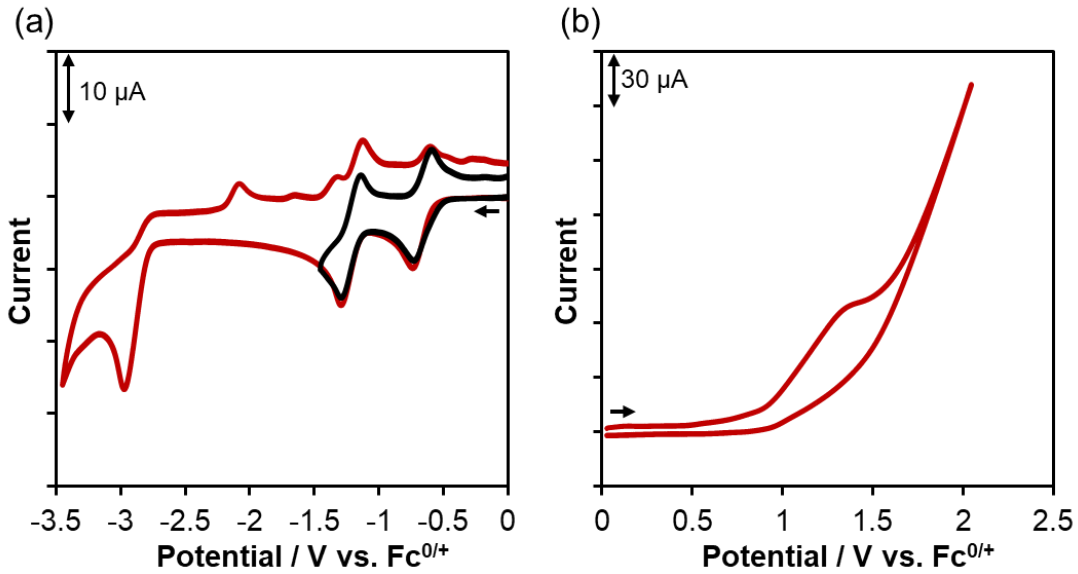

Figure S24 (a) The reduction waves and (b) the oxidation waves in cyclic voltammograms of [**2a**](OTf)$_2$ in a THF solution containing $TBAPF_6$ (0.1 M) as a supporting electrolyte at a sweep rate of 100 mV s^{-1} under N_2. A glassy carbon electrode (diameter: 3 mm) and a Pt wire were used as working and counter electrodes, respectively. All potentials were measured against an $Ag^{0/+}$ electrode and converted to the values *vs*. ferrocene/ferrocenium ($Fc^{0/+}$) referenced to an external standard ($Fc^{0/+}$). The scan was started (a) from 0.0 V to the negative direction or (b) from 0.0 V to the positive direction.

The voltammogram shown in (a) contained two reversible waves at −0.66 and −1.22 V, meaning that [**2a**](OTf)$_2$ can accept electrons from **3a*** (E_{ox}*: −2.15 V) to result in promoting the charge recombination processes. An irreversible oxidation wave was observed from around +1 V in (b), meaning that the unexpected oxidation of [**2a**](OTf)$_2$ by **3a**$^+$ (E_{ox}: +0.27 V) hardly proceeded in the photocatalytic reactions.

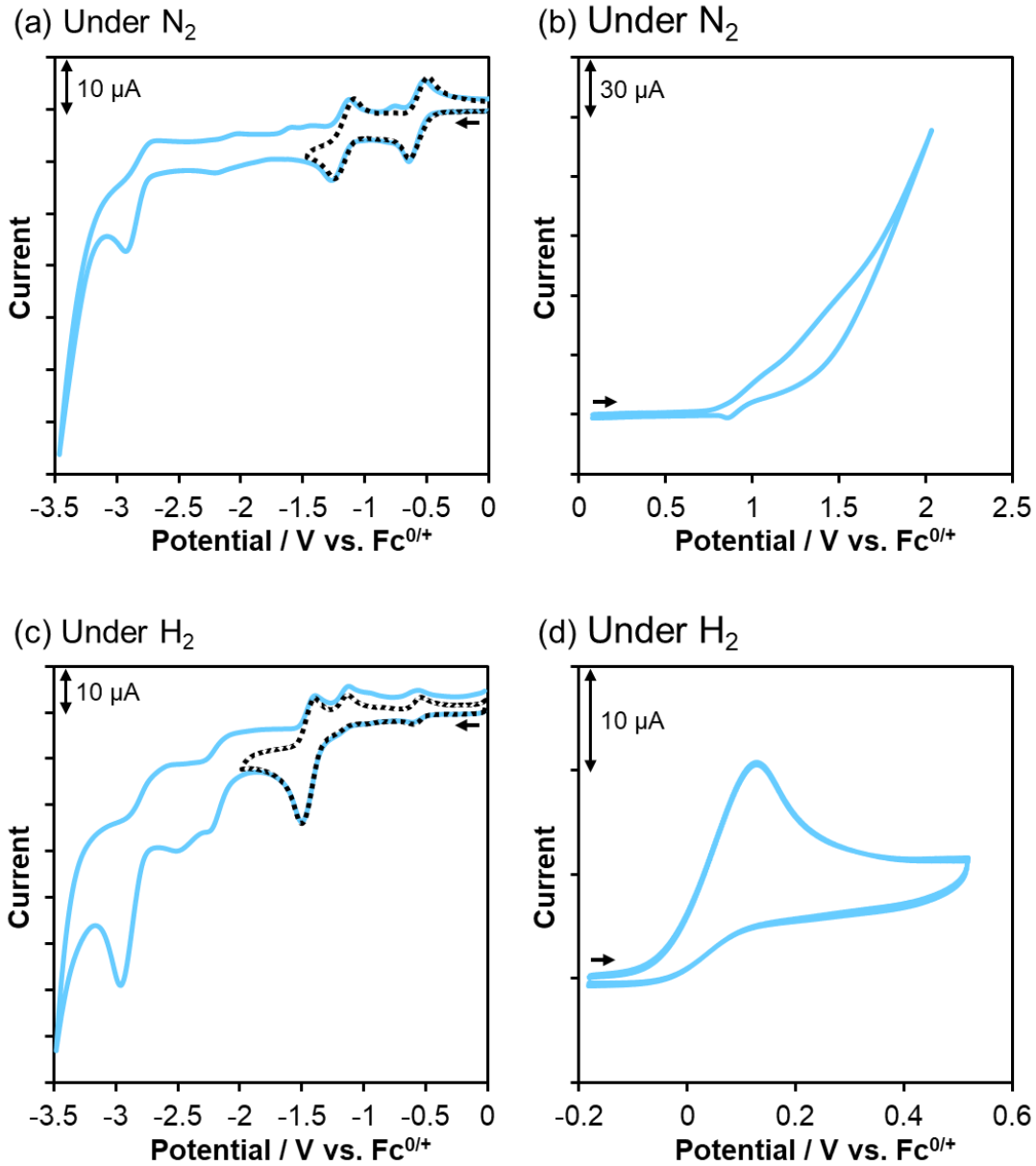

Figure S25 (a) The reduction waves and (b) the oxidation waves in cyclic voltammograms of [**2b**](OTf)$_2$ in a THF solution containing TBAPF$_6$ (0.1 M) as a supporting electrolyte at a sweep rate of 100 mV s^{-1} under N$_2$. The voltammograms measured after bubbling with H$_2$ gas for 1 h are illustrated in (c) and (d). A glassy carbon electrode (diameter: 3 mm) and a Pt wire were used as working and counter electrodes, respectively. All potentials were measured against an Ag$^{0/+}$ electrode and converted to the values *vs*. ferrocene/ferrocenium (Fc$^{0/+}$) referenced to an external standard (Fc$^{0/+}$). The scan was started (a) from +0.1 V to the negative direction, (b) from +0.1 V to the positive direction, (c) from 0.0 V to the negative direction, or (d) from −0.2 V to the positive direction.

The voltammogram under N$_2$ shown in (a) contained two reversible waves at −0.56 and −1.16 V, meaning that [**2b**](OTf)$_2$ can accept electrons from **3a*** (E_{ox}*: −2.15 V) to result in promoting the charge recombination processes. The voltammogram under N$_2$ shown in (b) contained an irreversible oxidation wave from around +0.9 V, meaning that the unexpected oxidation of [**2b**](OTf)$_2$ by **3a**$^+$ (E_{ox}: +0.27 V) hardly proceeded in the photocatalytic hydrogenation of **1a**.

The voltammogram under H$_2$ shown in (c) contained a quasi-reversible wave at −1.50 V and several irreversible waves, meaning that the hydride complex, which was produced from [**2b**](OTf)$_2$ under H$_2$, was possibly decomposed by the electron transfer from **3a*** (E_{ox}*: −2.15 V). These decomposition reactions might have led to the low durability of the photocatalytic reaction with [**2b**](OTf)$_2$ (Table S3). The voltammogram under H$_2$ shown in (d) contained an irreversible oxidation wave at +0.13 V, meaning that the one-electron-oxidized species of **3a** (**3a**$^+$, E_{ox}: +0.27 V) can oxidize the hydride complex, which was produced from [**2b**](OTf)$_2$ under H$_2$, to trigger the catalytic cycle for dihydrogen oxidation.

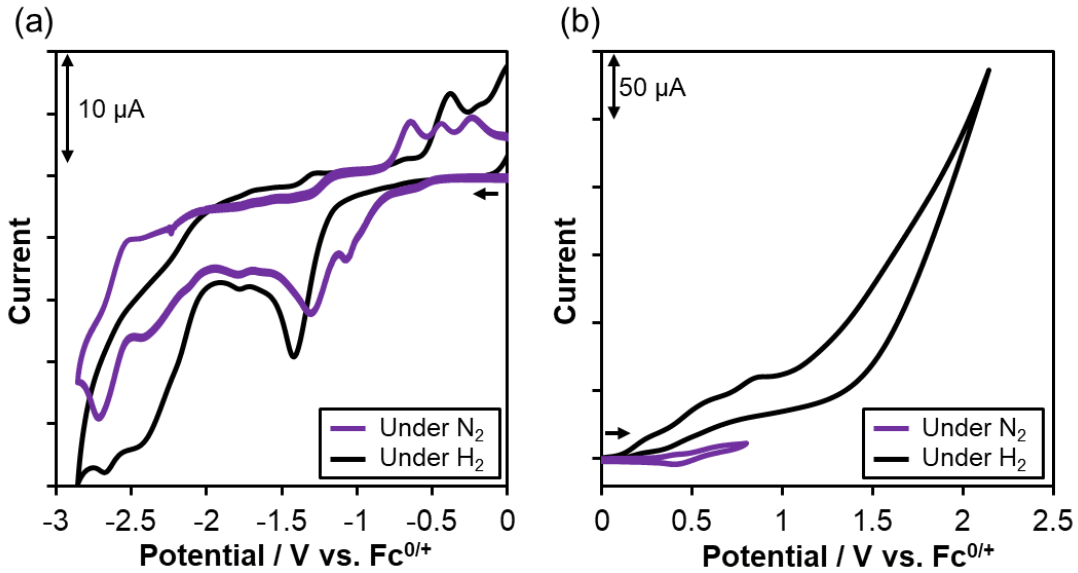

Figure S26 (a) The reduction waves and (b) the oxidation waves in cyclic voltammograms of [**2c**](OTf)$_2$ in a THF solution containing TBAPF$_6$ (0.1 M) as a supporting electrolyte at a sweep rate of 100 mV s^{-1} under N_2 (violet). The voltammograms measured after bubbling with H_2 gas for 1 h are illustrated in the black line. A glassy carbon electrode (diameter: 3 mm) and a Pt wire were used as working and counter electrodes, respectively. All potentials were measured against an Ag$^{0/+}$ electrode and converted to the values *vs*. ferrocene/ferrocenium (Fc$^{0/+}$) referenced to an external standard (Fc$^{0/+}$). The scan was started (a) from +0.1 V to the negative direction or (b) from 0.0 V to the positive direction.

The voltammogram under N_2 shown in (a) contained several irreversible waves, meaning that [**2c**](OTf)$_2$ was possibly decomposed by the electron transfer from **3a*** (E_{ox}*: −2.15 V). The voltammogram under N_2 shown in (b) did not contain any oxidation wave between 0 and 0.8 V, meaning that the unexpected oxidation of [**2c**](OTf)$_2$ by **3a**$^+$ (E_{ox}: +0.27 V) hardly proceeded in the photocatalytic hydrogenation of **1a**.

The voltammogram under H_2 shown in (a) contained several irreversible waves, meaning that the hydride complex, which was produced from [**2c**](OTf)$_2$ under H_2, was possibly decomposed by the electron transfer from **3a*** (E_{ox}*: −2.15 V). These decomposition reactions might have led to the low durability of the photocatalytic hydrogenation of **1a** with [**2c**](OTf)$_2$ (Table S4). The voltammogram under H_2 shown in (b) contained an irreversible oxidation wave (possibly catalytic wave) from around +0.2 V, meaning that the oxidation by the one-electron-oxidized species of **3a** (**3a**$^+$, E_{ox}: +0.27 V) can trigger oxidation of the hydride complex, which was produced from [**2c**](OTf)$_2$ under H_2, and the catalytic cycle for dihydrogen oxidation.

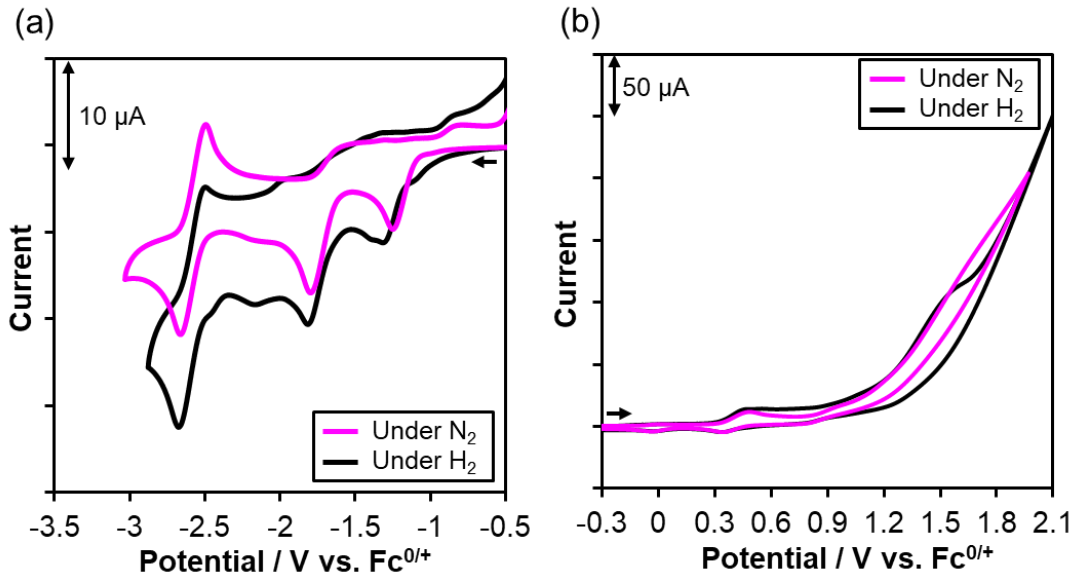

Figure S27 (a) The reduction waves and (b) the oxidation waves in cyclic voltammograms of [**2d**]OTf in a THF solution containing $TBAPF_6$ (0.1 M) as a supporting electrolyte at a sweep rate of 100 mV s^{-1} under N_2 (pink). The voltammograms measured after bubbling with H_2 gas for 1 h are illustrated in the black line. A glassy carbon electrode (diameter: 3 mm) and a Pt wire were used as working and counter electrodes, respectively. All potentials were measured against an $Ag^{0/+}$ electrode and converted to the values *vs*. ferrocene/ferrocenium ($Fc^{0/+}$) referenced to an external standard ($Fc^{0/+}$). The scan was started (a) from −0.4 V to the negative direction or (b) from −0.4 V to the positive direction.

The voltammogram under N_2 shown in (a) contained two irreversible waves at −1.26 and −1.79 V, and one reversible wave at −2.58 V, meaning that the molecular structure of [**2d**]OTf was probably changed by the electron transfer from **3a*** (E_{ox}*: −2.15 V) during reaction (the possible structural change should be the ligand substitution). The voltammogram under N_2 shown in (b) contained a quasi-reversible oxidation wave at +0.42 V, meaning that the unexpected oxidation of [**2d**]OTf by $\mathbf{3a}^+$ (E_{ox}: +0.27 V) possibly proceeded in the photocatalytic reactions.

The voltammograms under H_2 shown in (c) and (d) contained the same waves as those measured under N_2, and the shapes of the voltammograms remained almost unchanged even after bubbling with H_2 for another 1 h. These results suggest that most of the [**2d**]OTf did not react with H_2, although the small differences in the shapes of voltammograms might have been derived from the hydride complex, which was produced from [**2d**]OTf under H_2. This low reactivity of [**2d**]OTf with H_2 in THF might be a reason for the low efficiency of the photocatalytic hydrogenation of **1a** with [**2d**]OTf (Table S5).

Table S15. Electrochemical properties of the dihydrogen oxidation catalysts in THF. [a]

Complex	E_{ox} [V]	E_{red} [V]		
[**2a-H**]OTf	+0.24[b]	−1.58[c]	−2.24[c]	
[**2a**]$(OTf)_2$	—	−0.66[c]	−1.22[c]	−2.97[b]
[**2b**]$(OTf)_2$	—	−0.56[c]	−1.16[c]	−2.92[b]
Under H_2	+0.13[b]	−1.50[b]	−2.51[b]	−2.96[b]
[**2c**]$(OTf)_2$	—	−1.07[b]	−1.31[b]	−2.72[b]
Under H_2	—	−1.42[b]	−2.68[b]	
[**2d**]OTf	+0.42[c]	−1.26[b]	−1.79[b]	−2.58[c]

[a]Measured in a THF solution containing the complex (0.5 mM) and $TBAPF_6$ (0.1 M) with a scan rate of 100 mV s^{-1} under a N_2 atmosphere (Figures S23-27). [b]Peak potentials (E_p) vs. $Fc^{0/+}$. [c]Half-wave potentials ($E_{1/2}$) vs. $Fc^{0/+}$.

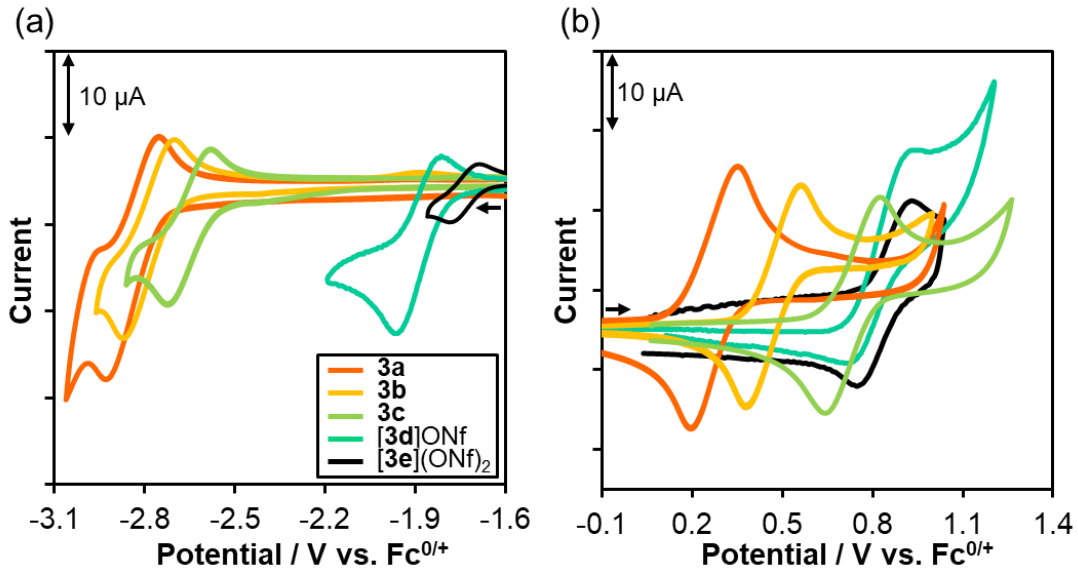

Figure S28. Cyclic voltammograms at (a) the first reduction waves and (b) the first oxidation waves of **3a** (orange), **3b** (yellow), **3c** (yellow green), [**3d**]ONf (light green), and [**3e**](ONf)$_2$ (black) in a THF solution containing TBAPF$_6$ (0.1 M) as a supporting electrolyte at a sweep rate of 100 mV s^{-1} under N$_2$. The sweep rate for measuring the oxidation waves of [**3e**](ONf)$_2$ was increased to 1000 mV s^{-1} because the wave became irreversible when the sweep rate was 100 mV s^{-1}. A glassy carbon electrode (diameter: 3 mm) and a Pt wire were used as working and counter electrodes, respectively. All potentials were measured against an Ag$^{0/+}$ electrode and converted to the values *vs.* ferrocene/ferrocenium (Fc$^{0/+}$) referenced to an external standard (Fc$^{0/+}$). The scan was started (a) from the following potentials (a) to the negative direction or (b) to the positive direction: **3a**, −0.4 V; **3b**, −0.2 V; **3c**, −0.5 V; [**3d**]ONf, −0.3 V; [**3e**](ONf)$_2$, −0.5 V.

Table S16. Electrochemical properties of the photosensitizers in THF. [a]

Photosensitizer	E_{red} [V] [b]	E_{ox} [V] [b]	$E_{0\text{-}0}$ [eV] [c]	E_{red}* [V] [d]	E_{ox}* [V] [d]
3a	−2.84	+0.27	2.42	−0.42	−2.15
3b	−2.76	+0.51	2.56	−0.20	−2.05
3c	−2.65	+0.73	2.64	−0.01	−1.91
[3d]ONf	−1.88	+0.83	2.22	+0.34	−1.39
[3e](ONf)$_2$	−1.77	+0.84 [e]	1.98	+0.21	−1.14

[a]Measured in a THF solution containing the complex (0.5 mM) and TBAPF$_6$ (0.1 M) with a scan rate of 100 mV s^{-1} under a N$_2$ atmosphere (Figure S28). [b]Half-wave potentials ($E_{1/2}$) vs. Fc$^{0/+}$. [c]Excitation energy determined by Franck-Condon analysis (Figure S18). [d]Redox potentials in the excited states calculated from E_{red}* = E_{red} + $E_{0\text{-}0}$ and E_{ox}* = E_{ox} − $E_{0\text{-}0}$. [e]The sweep rate was changed to 1000 mV s^{-1}.

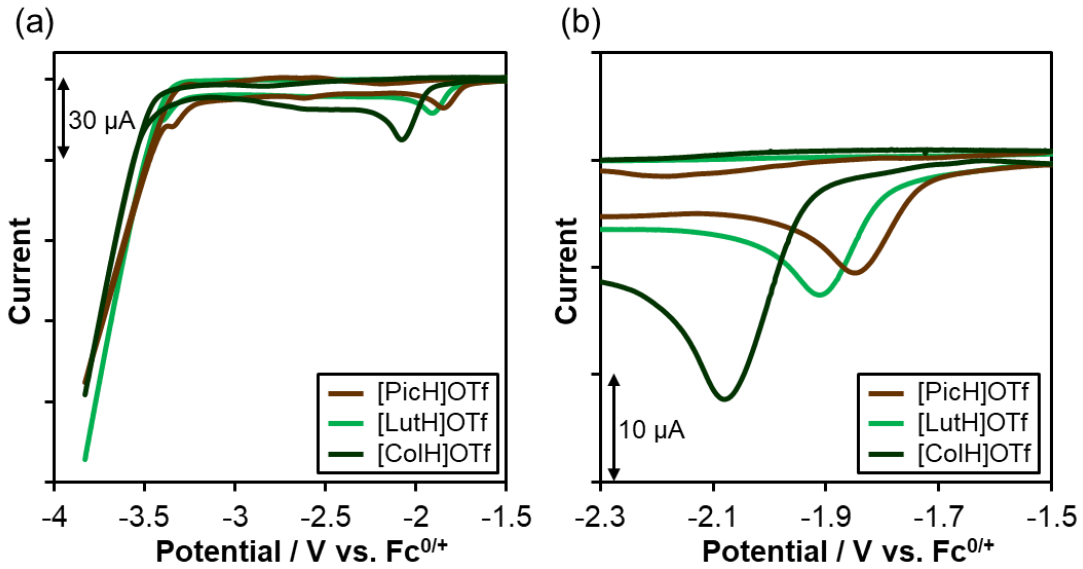

Figure S29. Cyclic voltammograms of [LutH]OTf (green), [ColH]OTf (dark green), and [PicH]OTf (brown) in a THF solution containing $TBAPF_6$ (0.1 M) as a supporting electrolyte at a sweep rate of 100 mV s^{-1} under N_2. The enlarged voltammograms are illustrated in (b). A glassy carbon electrode (diameter: 3 mm) and a Pt wire were used as working and counter electrodes, respectively. All potentials were measured against an $Ag^{0/+}$ electrode and converted to the values *vs*. ferrocene/ferrocenium ($Fc^{0/+}$) referenced to an external standard ($Fc^{0/+}$). The scan was started from −1.3 V to the negative direction.

Table S17. Electrochemical properties of the proton mediators in THF. [a]

Proton mediator	E_{red} [V] [b]
[LutH]OTf	−1.91
[ColH]OTf	−2.08
[PicH]OTf	−1.85

[a]Measured in a THF solution containing the complex (0.5 mM) and $TBAPF_6$ (0.1 M) with a scan rate of 100 mV s^{-1} under a N_2 atmosphere (Figure S29). [b]Peak potentials (E_p) vs. $Fc^{0/+}$.

5.3. Estimation of effective BDFE values

Table S18. The calculation of the effective BDFE value of the combination of **3a*** and $[LutH]^+$.

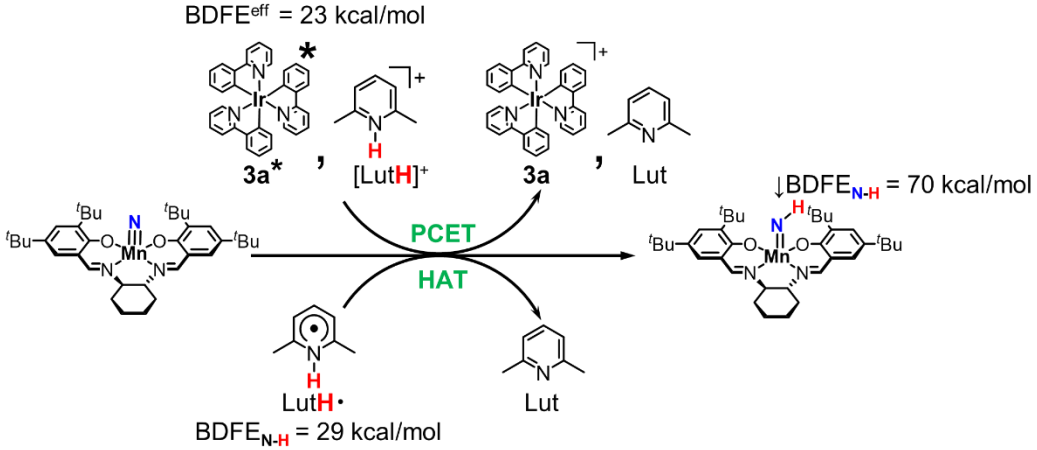

	Oxidation potential of electron donor [V]	pK_a of proton donor [c]	C_G [d] [kcal/mol]	$BDFE^{eff}$ [kcal/mol][e]
3a* and $[LutH]^+$	−2.15 [a]	9.5	59.9	23.2
$LutH^•$	−1.91 [b]	9.5	59.9	28.8

[a]The value from Table S16. [b]The value from Table S17. [c]The values from Supplementary Reference [24]. [d]C_G constants are derived from the solvent-dependent $H^+/H^•$ reduction potential. The values from Supplementary Reference [25]. [e]Effective bond dissociation free energy ($BDFE^{eff}$) calculated using the following equation:[14]

$BDFE^{eff} = 23.06\times(\text{Oxidation potential of electron donor}) + 1.36\times(pK_a \text{ of proton donor}) + C_G$ (S8)

The BDFE of the N-H bond in the imide complexes corresponding to **1a** was reported to be 70 kcal/mol,[26] suggesting that both the PCET and the HAT processes proceed exergonically.

6. Investigation on interaction between 1a-^{15}N and [LutH]OTf

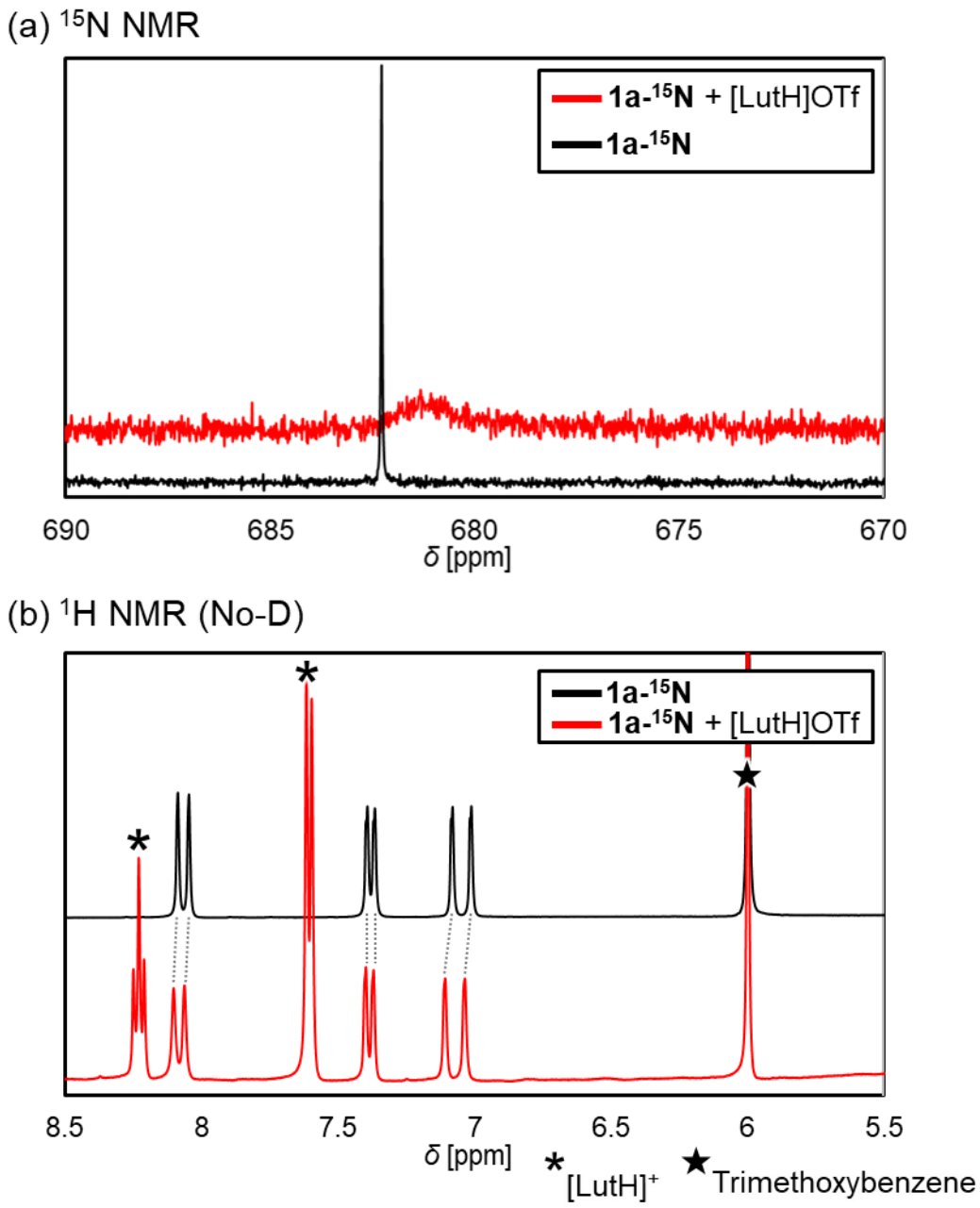

Figure S30. (a) ^{15}N NMR spectra and (b) No-Deuterium Proton (No-D) NMR spectra of **1a-^{15}N** (0.04 mM) in the presence of 1 mM [LutH]OTf (red lines). The solvent was THF. The intensity of the ^{15}N NMR spectrum in (a) was tripled for clarity. The spectra in the absence of [LutH]OTf are also illustrated in black lines for comparison. 1,3,5-Trimethoxybenzene (8.4 mg, 50 μmol) was added as an internal standard (δ in No-D NMR spectrum: 5.999 ppm).

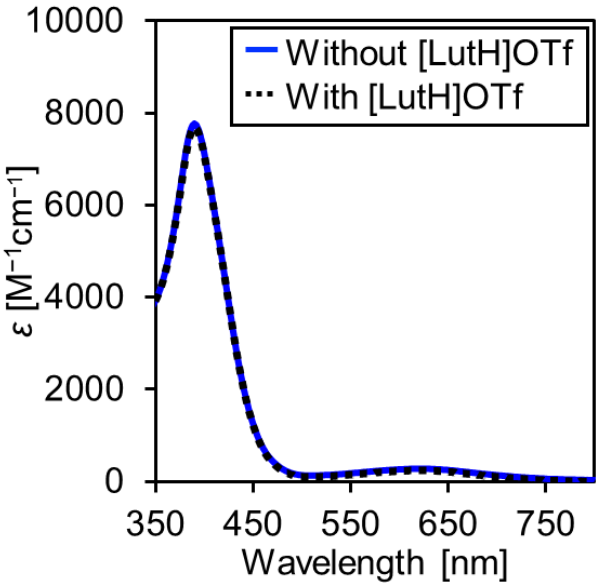

Figure S31. UV-vis absorption spectra of **1a** in the absence of [LutH]OTf (blue solid line) and in the presence of [LutH]OTf (1 equiv., black dotted line). The solvent is THF.

7. Supplementary references

1. Clarke, R. M.; Storr, T., Tuning Electronic Structure to Control Manganese Nitride Activation. *J. Am. Chem. Soc.* **2016**, *138*, 15299-15302.
2. Du Bois, J.; Hong, J.; Carreira, E. M.; Day, M. W., Nitrogen Transfer from a Nitridomanganese(V) Complex: Amination of Silyl Enol Ethers. *J. Am. Chem. Soc.* **1996**, *118*, 915-916.
3. Hein, N. M.; MacNeil, G. A.; Storr, T., Elaboration on the Electronics of Salen Manganese Nitrides: Investigations into Alkoxy-Substituted Ligand Scaffolds. *Inorg. Chem.* **2021**, *60*, 16895-16905.
4. Yuki, M.; Sakata, K.; Hirao, Y.; Nonoyama, N.; Nakajima, K.; Nishibayashi, Y., Thiolate-Bridged Dinuclear Ruthenium and Iron Complexes as Robust and Efficient Catalysts toward Oxidation of Molecular Dihydrogen in Protic Solvents. *J. Am. Chem. Soc.* **2015**, *137*, 4173-4182.
5. Yuki, M.; Sakata, K.; Nakajima, K.; Kikuchi, S.; Sekine, S.; Kawai, H.; Nishibayashi, Y., Dicationic Thiolate-Bridged Diruthenium Complexes for Catalytic Oxidation of Molecular Dihydrogen. *Organometallics* **2017**, *36*, 4499-4506.
6. Yuki, M.; Sakata, K.; Kikuchi, S.; Kawai, H.; Takahashi, T.; Ando, M.; Nakajima, K.; Nishibayashi, Y., Catalytic Activity of Thiolate-Bridged Diruthenium Complexes Bearing Pendent Ether Moieties in the Oxidation of Molecular Dihydrogen. *Chem. Eur. J.* **2017**, *23*, 1007-1012.
7. Pfund, B.; Steffen, D. M.; Schreier, M. R.; Bertrams, M. S.; Ye, C.; Borjesson, K.; Wenger, O. S.; Kerzig, C., Uv Light Generation and Challenging Photoreactions Enabled by Upconversion in Water. *J. Am. Chem. Soc.* **2020**, *142*, 10468-10476.
8. Miyake, Y.; Ashida, Y.; Nakajima, K.; Nishibayashi, Y., Visible-Light-Mediated Addition of Alpha-Aminoalkyl Radicals to [60]Fullerene by Using Photoredox Catalysts. *Chem. Eur. J.* **2014**, *20*, 6120-6125.
9. DiCiccio, A. M.; Longo, J. M.; Rodriguez-Calero, G. G.; Coates, G. W., Development of Highly Active and Regioselective Catalysts for the Copolymerization of Epoxides with Cyclic Anhydrides: An Unanticipated Effect of Electronic Variation. *J. Am. Chem. Soc.* **2016**, *138*, 7107-13.
10. Arashiba, K.; Kinoshita, E.; Kuriyama, S.; Eizawa, A.; Nakajima, K.; Tanaka, H.; Yoshizawa, K.; Nishibayashi, Y., Catalytic Reduction of Dinitrogen to Ammonia by Use of Molybdenum-Nitride Complexes Bearing a Tridentate Triphosphine as Catalysts. *J. Am. Chem. Soc.* **2015**, *137*, 5666-5669.
11. Arashiba, K.; Miyake, Y.; Nishibayashi, Y., A Molybdenum Complex Bearing PNP-Type Pincer Ligands Leads to the Catalytic Reduction of Dinitrogen into Ammonia. *Nat. Chem.* **2011**, *3*, 120-125.
12. Weatherburn, M. W., Phenol-Hypochlorite Reaction for Determination of Ammonia. *Anal. Chem.* **1967**, *39*, 971-974.
13. Hatchard, C. G.; Parker, C. A., A New Sensitive Chemical Actinometer - II. Potassium Ferrioxalate as a Standard Chemical Actinometer. *Proc. R. Soc. A.* **1956**, *235*, 518-536.
14. Stoll, S.; Schweiger, A., Easyspin, a Comprehensive Software Package for Spectral Simulation and Analysis in EPR. *J. Magn. Reson.* **2006**, *178*, 42-55.
15. Kar, A. K.; Acharya, A.; Pradhan, G. C.; Dash, A. C., Glyoxylate as a Reducing Agent for Manganese(III) in Salen Scaffold: A Kinetics and Mechanistic Study. *J. Chem. Sci.* **2014**, *126*, 547-559.
16. Wang, D.; Loose, F.; Chirik, P. J.; Knowles, R. R., N-H Bond Formation in a Manganese(V) Nitride Yields Ammonia by Light-Driven Proton-Coupled Electron Transfer. *J. Am. Chem. Soc.* **2019**, *141*, 4795-4799.
17. Kim, S.; Zhong, H.; Park, Y.; Loose, F.; Chirik, P. J., Catalytic Hydrogenation of a Manganese(V) Nitride to Ammonia. *J. Am. Chem. Soc.* **2020**, *142*, 9518-9524.
18. CrysAlisPro: version 1.171.41.99a, Data Collection and Processing Software; Rigaku Corporation: Tokyo, Japan, **2021**.
19. CrystalStructure 4.3: Crystal Structure Analysis Package, Rigaku Corporation, Tokyo, Japan, **2019**.
20. Sheldrick, G. M. SHELXT – Integrated Space-Group and Crystal-Structure Determination. *Acta Crystallogr. Sect. Found. Adv.* **2015**, *71*, 3–8.
21. Sheldrick, G. M. Crystal Structure Refinement with SHELXL. *Acta Crystallogr. Sect. C Struct. Chem.* **2015**, *71*, 3–8.
22. Spek, A. L., Platon Squeeze: A Tool for the Calculation of the Disordered Solvent Contribution to the Calculated Structure Factors. *Acta Crystallogr. C* **2015**, *71*, 9-18.
23. Allen, G. H.; White, R. P.; Rillema, D. P.; Meyer, T. J., Synthetic Control of Excited-State Properties. Tris-Chelate Complexes Containing the Ligands 2,2'-Bipyrazine, 2,2'-Bipyridine, and 2,2'-Bipyrimidine. *J. Am. Chem Soc.* **1984**, *106*, 2613-2620.
24. Tanabe, Y.; Nishibayashi, Y., Comprehensive Insights into Synthetic Nitrogen Fixation Assisted by Molecular Catalysts under Ambient or Mild Conditions. *Chem. Soc. Rev.* **2021**, *50*, 5201-5242.
25. Agarwal, R. G.; Coste, S. C.; Groff, B. D.; Heuer, A. M.; Noh, H.; Parada, G. A.; Wise, C. F.; Nichols, E. M.; Warren, J. J.; Mayer, J. M., Free Energies of Proton-Coupled Electron Transfer Reagents and Their Applications. *Chem. Rev.* **2022**, *122*, 1-49.
26. Panetti, G. B.; Kim, J.; Myong, M. S.; Bird, M. J.; Scholes, G. D.; Chirik, P. J., Photodriven Ammonia Synthesis from Manganese Nitrides: Photophysics and Mechanistic Investigations. *J. Am. Chem. Soc.* **2024**, *146*, 27610-27621.